




# Robust *ab initio* predictions for dimensionless ratios of $E2$ and radius observables.

## II. Estimation of $E2$ transition strengths by calibration to the charge radius

Mark A. Caprio <sup>1</sup>, Patrick J. Fasano <sup>1,2,\*</sup> and Pieter Maris <sup>3</sup>

<sup>1</sup>*Department of Physics and Astronomy, University of Notre Dame, Notre Dame, Indiana 46556-5670, USA*

<sup>2</sup>*Physics Division, Argonne National Laboratory, Argonne, Illinois 60439-4801, USA*

<sup>3</sup>*Department of Physics and Astronomy, Iowa State University, Ames, Iowa 50011-3160, USA*

(Dated: January 17, 2025)

Converged results for  $E2$  observables are notoriously challenging to obtain in *ab initio* no-core configuration interaction (NCCI) approaches. Matrix elements of the  $E2$  operator are sensitive to the large-distance tails of the nuclear wave function, which converge slowly in an oscillator basis expansion. Similar convergence challenges beset *ab initio* prediction of the nuclear charge radius. However, we exploit systematic correlations between the calculated  $E2$  and radius observables to yield meaningful predictions for relations among these observables. In particular, we examine *ab initio* predictions for dimensionless ratios of the form  $B(E2)/(e^2r^4)$ , for nuclei throughout the  $p$  shell. Meaningful predictions for  $E2$  transition strengths may then be made by calibrating to the ground-state charge radius, if experimentally known.

### I. INTRODUCTION

Converged predictions for nuclear electric quadrupole ( $E2$ ) transition strengths are challenging to obtain in *ab initio* approaches [1–6]. Long-range observables, *i.e.*, those which are sensitive to the large-distance tails of the nuclear wave function, such as  $E2$  matrix elements, are slowly convergent in *ab initio* no-core configuration interaction (NCCI), or no-core shell-model (NCSM), calculations [7], as these tails are described only with difficulty in an oscillator-basis expansion.

Nonetheless, one may exploit systematic correlations among calculated observables to yield meaningful predictions for relations among these observables, even where the observables individually are not adequately converged (*e.g.*, Refs. [8, 9]). Perhaps most naturally, the convergence patterns of different calculated  $E2$  matrix elements may be strongly correlated with each other (*e.g.*, Refs. [8, 10–13]). In particular, the dimensionless ratio  $B(E2)/(eQ)^2$ , relating the  $E2$  strength to the quadrupole moment, is in many cases found to be robustly convergent [8, 10, 11, 14–17]. A meaningful prediction of the  $E2$  strength may then be obtained by calibration to a measured ground-state quadrupole moment [16].

However, correlations among the  $E2$  matrix elements are not the only ones which might be exploited. There are cases in which the ground-state quadrupole moment is not suitable for use in calibration, either since it is unknown, or since it is subject to large calculational uncertainties and/or sensitivity to the internucleon interaction (as for the suppressed quadrupole moment in  ${}^6\text{Li}$  [8, 25]), or, more simply, since only states with angular momentum  $J \geq 1$  admit a nonvanishing quadrupole moment. Thus, notably, calibration to the ground-state quadrupole moment is not possible for even-even nuclei,

nor for odd-mass nuclei with  $J = 1/2$  ground states. (On a nuclear chart of the  $p$  shell, in Fig. 1, such nuclides are crossed out with a diagonal line.)

The electric monopole ( $E0$ ) and  $E2$  operators have a

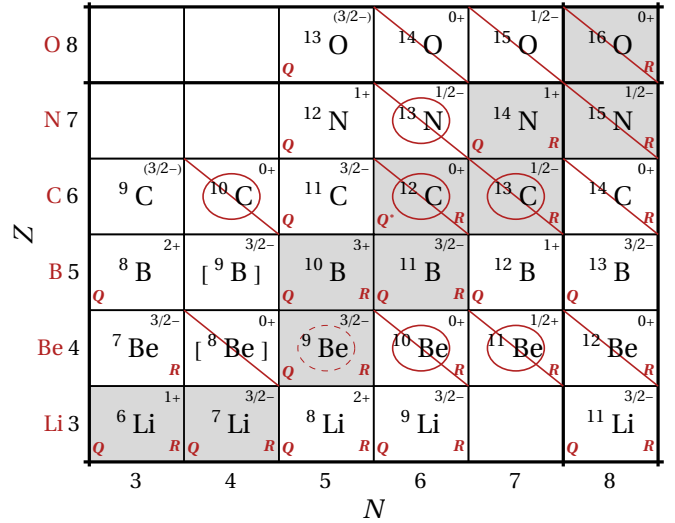


FIG. 1. Overview of particle-bound nuclides in the  $p$  shell, highlighting nuclides for which  $E2$  strengths are considered, in relation to the radius, in this work: the nuclide  ${}^9\text{Be}$  (dashed circle), for which the ground-state angular momentum *does* also support a quadrupole moment, and the remaining nuclides (solid circle), for which it does *not*. Nuclides with measured ground-state quadrupole moments [18] and charge radii [19, 20] are indicated by the letter “Q” or “R”, respectively, while a measured excited-state quadrupole moment [18] is indicated by “Q\*”. Brackets indicate a particle-unbound but narrow ( $\lesssim 1$  keV) ground-state resonance, shading indicates beta-stable nuclides, and the experimental ground-state angular momentum and parity are given [20–24]. Nuclei for which the ground-state angular momentum does not support a quadrupole moment ( $J \leq 1/2$ ) are crossed out with a diagonal line.

\* Present address: NextSilicon Inc., Minneapolis, Minnesota 55402-1572, USA

similar sensitivity ( $\propto r^2$ ) to the large-distance behavior of the nucleons in the nuclear many-body wave function. Therefore, we might hope to find  $E2$  observables also to be correlated with the  $E0$  moment or, equivalently, root mean square (r.m.s.) radius. If the dimensionless ratio  $B(E2)/(e^2r^4)$ , now involving the ground-state radius, is robustly convergent, then a meaningful prediction of the  $E2$  strength may again be obtained, now by calibration to a measured ground state (charge) radius.

Notionally, at least, these different dimensionless ratios,  $B(E2)/(eQ)^2$  and  $B(E2)/(e^2r^4)$ , are sensitive to different aspects of nuclear structure. In simple model limits [26], the ratio  $B(E2)/(eQ)^2$  is uniquely determined by symmetry considerations. *E.g.*, taking the axially symmetric rotor as a principal example,  $B(E2)/(eQ)^2$  follows from the rotational relations among electromagnetic matrix elements [27], independent of the magnitude of the nuclear quadrupole deformation. The ratio  $B(E2)/(e^2r^4)$ , instead, provides a measure of this deformation. In this same rotational picture, it is proportional to the square of the Bohr deformation variable  $\beta$  [28].

In a previous article (Part I) [29], we considered the relation between calculated  $E2$  and  $E0$  moments in the ground state, namely, through the dimensionless ratio  $Q/r^2$ . We did so for nuclei across the  $p$  shell. (If  $Q/r^2$  is robustly convergent, then a meaningful prediction of the quadrupole moment may be obtained, by calibration to a measured ground state radius, or *vice versa*.) The reader is also referred to Part I for background on the relation of such ratios to the quadrupole deformation, as well as the distinction between the point-proton radius  $r_p$  considered in nuclear structure calculations and the measurable charge radius  $r_c$ .

In the present article (Part II), we address  $E2$  transition strengths, through the dimensionless ratio  $B(E2)/(e^2r^4)$ , for low-lying  $E2$  transitions in selected  $p$ -shell nuclei. We focus primarily on nuclei for which the ground state does not support a quadrupole moment (that is, nuclei for which calibration to the ground-state radius is, at least in principle, possible, while calibration to the quadrupole moment is not).

First, we compare the convergence properties of the dimensionless ratios  $B(E2)/(eQ)^2$  and  $B(E2)/(e^2r^4)$ , taking for illustration a nuclide for which the ground-state angular momentum *does* support a quadrupole moment, namely,  ${}^9\text{Be}$  [Fig. 1 (dashed circle)] (Sec. II). We then relate the  $E2$  strength to the radius, via  $B(E2)/(e^2r^4)$ , for transitions in  $p$ -shell nuclei for which the ground-state angular momentum *does not* support a quadrupole moment (Sec. III): namely, the even-even ( $J = 0$ ) nuclides  ${}^{10}\text{Be}$ ,  ${}^{10}\text{C}$ , and  ${}^{12}\text{C}$ , and the odd-mass ( $J = 1/2$ ) nuclides  ${}^{11}\text{Be}$ ,  ${}^{13}\text{C}$ , and  ${}^{13}\text{N}$  [Fig. 1 (solid circles)]. We also consider dimensionless ratios  $B(E2)/(eQ)^2$ , involving the quadrupole moment of the excited initial state for the transition, as a diagnostic for axially symmetric rotational structure, as well as  $Q/r^2$  for the experimentally measured  $2^+$  quadrupole moment of  ${}^{12}\text{C}$  [18, 30, 31]. Finally, we use these results to extract the deformations

of the proton and neutron distributions of the nuclear intrinsic state, under the assumption of axial symmetry (Sec. IV). Preliminary results were reported in Ref. [32].

## II. CONVERGENCE ILLUSTRATION: CALIBRATION TO THE QUADRUPOLE MOMENT AND RADIUS IN ${}^9\text{Be}$

As an illustrative example, let us take the lowest lying  $E2$  transition in  ${}^9\text{Be}$ , that is, the  $5/2^- \rightarrow 3/2^-$  transition from the first negative parity excited state to the ground state. We have already examined the convergence of the ground state quadrupole moment and radius, and the dimensionless ratio  $Q/r^2$  involving these, in Sec. III of Part I. Although the  $5/2^-$  state, at 2.42 MeV, lies above the neutron threshold, it is a narrow resonance, with a width of  $\approx 0.8$  keV [22]. The  $3/2^-$  ground state may be interpreted as the band head of a  $K = 3/2$  rotational band [34–36], and the  $5/2^-$  state as a band member, so that the  $5/2^- \rightarrow 3/2^-$  transition is a rotational in-band transition (see Fig. 1 of Ref. [36]). The  $E2$  strength for this transition is measured experimentally as  $B(E2; 5/2^- \rightarrow 3/2^-) = 28(2) e^2\text{fm}^4$  [22].

Calculated observables pertaining to this  $5/2^- \rightarrow 3/2^-$  transition in  ${}^9\text{Be}$  are shown in Fig. 2. Each curve in Fig. 2 represents the results of calculations sharing the same truncation  $N_{\text{max}}$ , for the many-body harmonic oscillator basis, but with varying choices of the oscillator scale parameter  $\hbar\omega$  [7], as described in Part I. Calculations are carried out using the NCCI code MFDn [37] and the associated postprocessor code for transitions [38].

In Fig. 2, we take NCCI calculations based on three different internucleon interactions (left to right), as described in Part I: Daejeon16 [39], JISP16 [40], and a chiral effective field theory ( $\chi\text{EFT}$ ) interaction, namely, the two-body part of the  $\text{N}^2\text{LO}$  LENPIC interaction (with semi-local coordinate-space regulator parameter  $R = 1$  fm) [41, 42]. Of these, the Daejeon16 interaction is the “softest”, providing the most favorable convergence properties, while the LENPIC interaction is the “hardest”, since here it is taken with no similarity renormalization group (SRG) softening. Also shown in Fig. 2 are experimental values (squares) and the predictions of Green’s function Monte Carlo (GFMC) calculations [33] with the Argonne  $v_{18}$  (AV18) two-nucleon [43] and Illinois-7 (IL7) three-nucleon [44] potentials (crosses).

The  $5/2^-$  excitation energy (*i.e.*, the energy difference for the  $5/2^- \rightarrow 3/2^-$  transition) is shown in Fig. 2 (first row). We note rough consistency in the scale of the excitation energy, both across the different calculations, and with experiment.

Before proceeding to the  $E2$  transition strength, it is worth recalling from Part I the convergence behaviors of the calculated ground state quadrupole moment  $Q$  and proton radius  $r_p$ . For the reader’s convenience, we replicate in Fig. 3 illustrative results for  $Q$ ,  $r_p$ , and  $Q/r_p^2$ , for the Daejeon16 interaction [from Fig. 2 (d.g.j) of Part I].

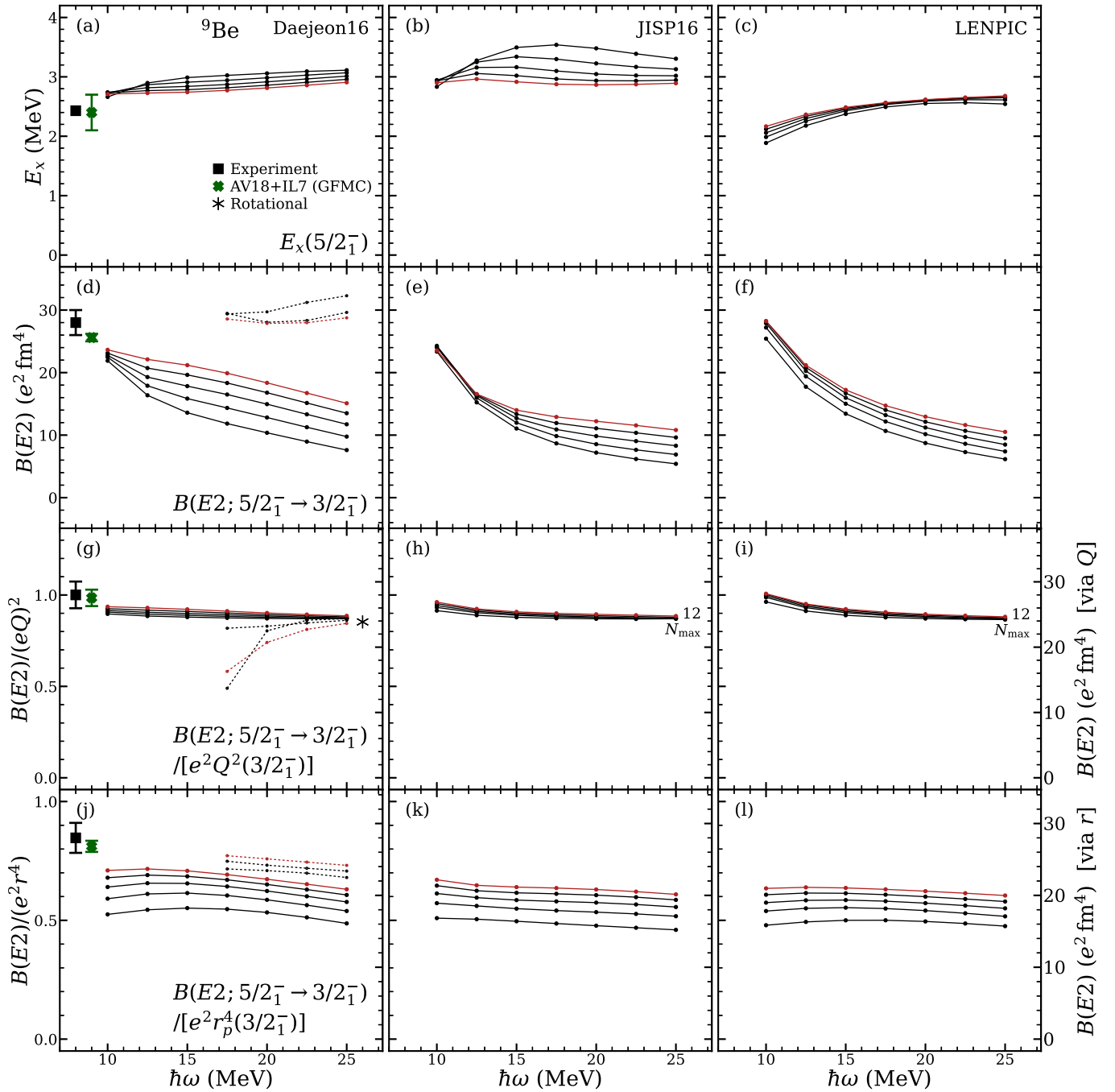


FIG. 2. Calculated transition observables for  ${}^9\text{Be}$ :  $E_x(5/2^-)$ ,  $B(E2; 5/2_1^- \rightarrow 3/2_1^-)$ , the dimensionless ratio  $B(E2)/(eQ)^2$ , and the dimensionless ratio  $B(E2)/(e^2 r_p^4)$  (from top to bottom). Results are shown for the Daejeon16 (left), JISP16 (center), and LENPIC (right) interactions. Calculated values are shown as functions of the basis parameter  $\hbar\omega$ , for successive even values of  $N_{\text{max}}$ , from  $N_{\text{max}} = 4$  to 12 (as labeled). When calibrated to the experimentally deduced value for  $Q$  or  $r_p$ , the ratio provides a prediction for the absolute  $B(E2)$  (scale at right). Exponential extrapolations (small circles, dotted lines) are provided, for selected observables, for the Daejeon16 results only ( $\hbar\omega \geq 17.5$  MeV). For comparison, experimental values [18, 19, 22] (squares), GFMC AV18+IL7 predictions [33] (see also Table III of Ref. [4] for  $E_x$ ) (crosses), and the rotational  $E2$  ratio (asterisk) are also shown. Includes results for  $B(E2)/(eQ)^2$  previously shown (for  $N_{\text{max}} \leq 10$ ) in Ref. [16].

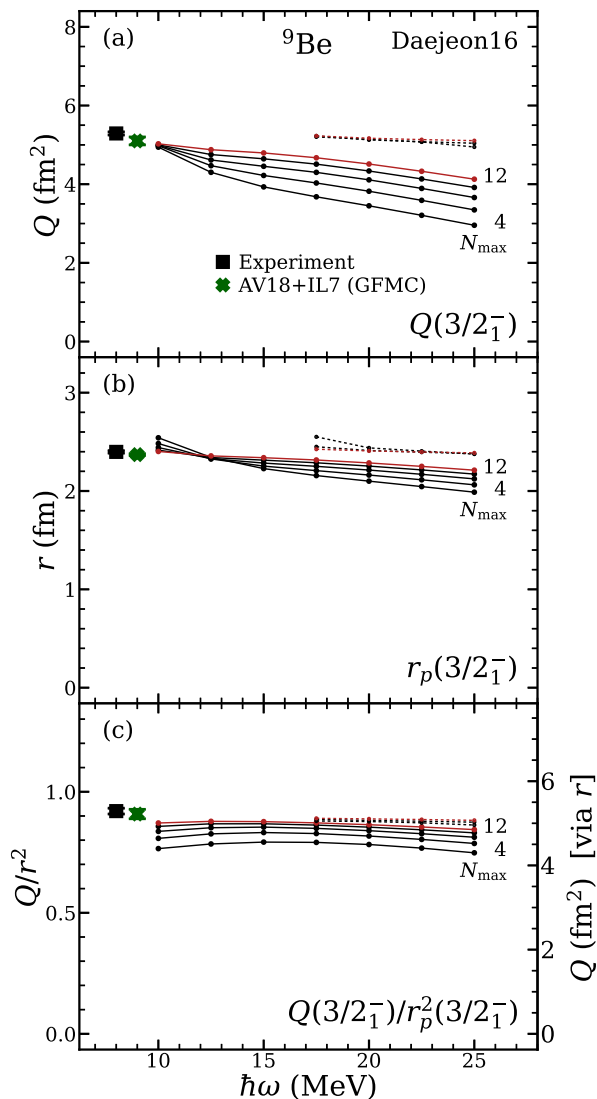


FIG. 3. Calculated ground state observables for  ${}^9\text{Be}$ : (a)  $Q(3/2^-)$ , (b)  $r_p(3/2^-)$ , and (c) the dimensionless ratio  $Q/r_p^2$ . Results are shown for the Daejeon16 interaction. Calculated values are shown as functions of the basis parameter  $\hbar\omega$ , for successive even values of  $N_{\text{max}}$ , from  $N_{\text{max}} = 4$  to 12 (as labeled). When calibrated to the experimentally deduced value for  $r_p$ , the ratio provides a prediction for the absolute  $Q$  (scale at right). Exponential extrapolations (small circles, dotted lines) are provided ( $\hbar\omega \geq 17.5$  MeV). For comparison, experimental values [18, 19] (squares) and GFMC AV18+IL7 predictions [33] (crosses) are also shown. Results reproduced from Fig. 2 of Part I.

For both  $Q$  [Fig. 3(a)] and  $r_p$  [Fig. 3(b)], we see a flattening (shouldering) of the curves, in the lower portion of the  $\hbar\omega$  range shown, and the spacing between curves for successive  $N_{\text{max}}$  decreases. While this behavior suggests an approach to convergence, the level of convergence is not sufficient for us to read off a concrete estimate of the true result for the observable in the full, untruncated space. (For the harder JISP16 and LENPIC interactions,

any such hints of convergence, especially shouldering, are less obvious.) For  $Q$ , the curves appear to approximately cross at a single point at or near the low end of the  $\hbar\omega$  range shown, or, for  $r_p$ , at a point somewhat higher in  $\hbar\omega$  (by  $\approx 2.5$  MeV). Then, taking the ratio  $Q/r_p^2$  [Fig. 3(c)] removes much of the  $N_{\text{max}}$  and  $\hbar\omega$  dependence observed for  $Q$ , although some  $\hbar\omega$  dependence remains (specifically, for the Daejeon16 results, taking the form of a gentle fall-off on either side of  $\hbar\omega \approx 15$  MeV).

Turning now to the present transition of interest, the calculated  $B(E2; 5/2^- \rightarrow 3/2^-)$  is shown in Fig. 2 (second row). For the results obtained with the Daejeon16 interaction [Fig. 2(d)], this quantity likewise shows some indication of shouldering in the lower portion of the  $\hbar\omega$  range shown, as well as some slight indication of compression with increasing  $N_{\text{max}}$  in the shouldering region. Again, there is no way to read off the true, converged value from these results with any confidence. Regarding the other, harder interactions, there is little sign of convergence (either compression of the curves or shouldering) in the calculated  $B(E2)$  for JISP16 [Fig. 2(e)] and essentially none for the bare LENPIC interaction [Fig. 2(f)].

We begin our consideration of dimensionless ratios with  $B(E2)/(eQ)^2$ , a ratio involving only  $E2$  matrix elements, as proposed in Ref. [16]. The calculated results for this ratio are shown for  ${}^9\text{Be}$  in Fig. 2 (third row). (Calibrating to the experimental ground state quadrupole moment [18] gives the scale shown at right.) The  $\hbar\omega$  dependence seen in the  $B(E2)$  [Fig. 2 (second row)] is essentially eliminated in the ratio  $B(E2)/(eQ)^2$ , and convergence with  $N_{\text{max}}$  is remarkably rapid. For the Daejeon16 results [Fig. 2(g)], the values obtained for successive  $N_{\text{max}}$  differ by  $\lesssim 1.5\%$  even for the lowest  $N_{\text{max}}$  shown. These Daejeon16 results lie just below the experimental ratio (square) and GFMC AV18+IL7 predictions [33] (cross) for the ratio, and just above (by  $\approx 5\%$ ) the  $K = 3/2$  rotational value [ $B(E2)/(eQ)^2 = 75/(28\pi) \approx 0.8526$ ] (asterisk).

However, our principal interest here is in the dimensionless ratio  $B(E2)/(e^2 r_p^4)$ , shown for  ${}^9\text{Be}$  in Fig. 2 (fourth row). (Calibrating to the experimental ground state point-proton radius [19] gives the scale shown at right.) Taking this ratio again serves to eliminate much of the  $\hbar\omega$  dependence found in the  $B(E2)$  itself [Fig. 2 (second row)]. For the Daejeon16 results [Fig. 2(j)], there is still a modest  $\hbar\omega$  dependence, similar to that seen above for  $Q/r_p^2$  [Fig. 3(c)], though this is not seen in the results for the other interactions [Fig. 2(k,l)]. Taking the ratio reduces, but does not eliminate, the  $N_{\text{max}}$  dependence found for the  $B(E2)$  itself. We may note that there is no apparent crossing point for the  $B(E2)$ , with respect to  $N_{\text{max}}$ , in the  $\hbar\omega$  range shown [Fig. 2 (d)]. Therefore, it is already clear that the  $B(E2)$  cannot be *strictly* correlated, in a one-to-one relation, to either  $Q$  [Fig. 3(a)] or  $r_p$  [Fig. 3(b)]. What is most striking is the improvement obtained, by taking the ratio, for the harder interactions [Fig. 2(h,i)], where the underlying  $B(E2)$  [Fig. 2(e,f)] is

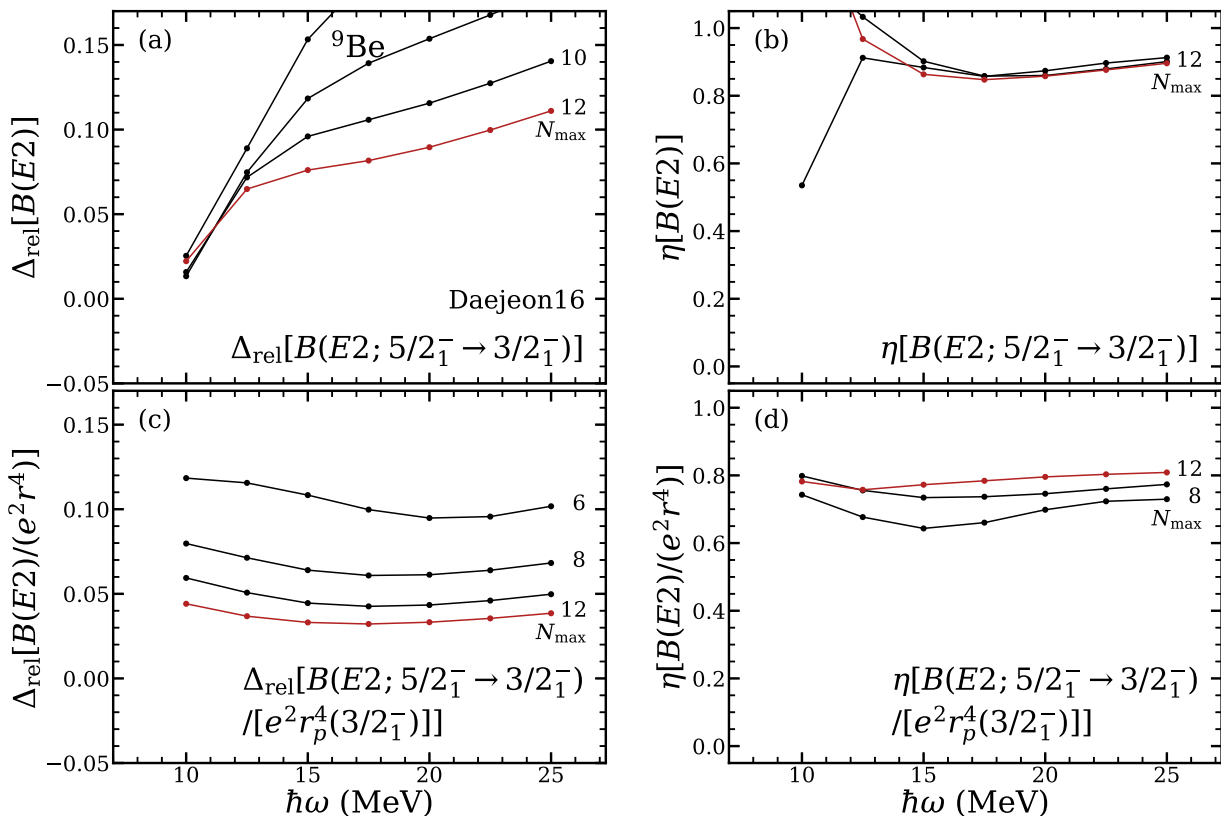


FIG. 4. Diagnostics of convergence for transition observables for  ${}^9\text{Be}$ : the relative difference  $\Delta_{\text{rel}}$  (left) and ratio of successive differences  $\eta$  (right), for  $B(E2; 5/2_1^- \rightarrow 3/2_1^-)$  (top) and the dimensionless ratio  $B(E2)/(e^2 r_p^4)$  (bottom). Calculated values, for the Daejeon16 interaction, are shown as functions of the basis parameter  $\hbar\omega$ , for successive even values of  $N_{\text{max}}$ , from  $N_{\text{max}} = 4$  to 12 (as labeled).

itself so poorly converged.<sup>1</sup>

At least in this example, the ratio  $B(E2)/(e^2 r_p^4)$  is not as robustly convergent as  $B(E2)/(eQ)^2$ . Nonetheless, it would still appear feasible to obtain a rough estimate (or at least a lower bound) for the  $B(E2)$  by calibration to the ground-state radius, using the *ab initio* calculations for this ratio in Fig. 2 (fourth row).

As in Part I, we may also consider quantitative measures of convergence, shown in Fig. 4 for both the  $B(E2)$  itself [Fig. 4 (top)] and the dimensionless ratio  $B(E2)/(e^2 r_p^4)$  [Fig. 4 (bottom)]. Namely, we show the relative differences  $\Delta_{\text{rel}}$  [Fig. 4 (left)], defined in (17) of Part I, and the ratio  $\eta$  of successive differences [Fig. 4 (right)], defined in (19) of Part I. For exponential convergence [2, 45], that is,  $N_{\text{max}}$  dependence of the form [see

(21) of Part I]

$$X(N_{\text{max}}) = X_{\infty} + a \exp(-cN_{\text{max}}),$$

an observable  $X$  approaches its limiting value in steps the sizes of which form a geometric progression. In this case,  $\eta$  should be constant with respect to  $N_{\text{max}}$ , at fixed  $\hbar\omega$ . In Part I, it was found (see Fig. 3 of Part I) that the ground state observables  $Q$  and  $r_p$  exhibit roughly exponential convergence with respect to  $N_{\text{max}}$ , in the  $\hbar\omega$  regions safely above any crossing point, but this convergence is slow, with  $\eta \approx 0.8$ .

For the  $B(E2)$ , the convergence is again seen to be roughly exponential, for the upper part of the  $\hbar\omega$  range shown ( $\hbar\omega \gtrsim 15$  MeV), in that  $\eta$  [Fig. 4 (b)] is approximately independent of  $N_{\text{max}}$ , at each  $\hbar\omega$ . The convergence rate, as measured by  $\eta$ , is weakly dependent on  $\hbar\omega$ . However, it is generally even slower ( $\eta \approx 0.9$ ) than for  $Q$  and  $r_p$ . For  $B(E2)/(e^2 r_p^4)$ , the relative differences [Fig. 4(c)] are no longer highly  $\hbar\omega$  dependent, as they are for the  $B(E2)$  itself [Fig. 4(a)]. The ratio of successive differences for  $B(E2)/(e^2 r_p^4)$  [Fig. 4(d)] is somewhat reduced ( $0.6 \lesssim \eta \lesssim 0.8$ ) relative to those for the  $B(E2)$  itself [Fig. 4 (b)], but this ratio is now more dependent upon  $N_{\text{max}}$ , signaling a convergence pattern which is less exponential. As noted in Part I, the ratio of two expo-

<sup>1</sup> Given the close proportionality between  $B(E2)$  and  $Q^2$  established above, note that the convergence properties of the ratio  $B(E2)/(e^2 r_p^4)$  found here [Fig. 2 (fourth row)] are largely foretold by those previously found (in Part I) for the ratio  $Q/r_p^2$  [Fig. 2 (bottom row) of Part I]. Since the numerator and denominator are now quadratic, rather than linear, in the underlying matrix elements (of the monopole and quadrupole operators), relative changes in  $B(E2)/(e^2 r_p^4)$  may be expected to be amplified by a factor of 2 compared to those in  $Q/r_p^2$ .

nentially converging quantities need not itself be exponentially converging (although it may be approximately so in limiting cases).

If we assume exponential convergence, on a purely empirical basis, we may extrapolate from values calculated at finite  $N_{\max}$  to the limiting value  $X_{\infty}$ . A simple three-point exponential extrapolation (see Appendix A of Part I) is given by the small circles and dotted curves in Figs. 2 and 3, for the Daejeon16 results. (From the calculations considered here, with  $N_{\max} \geq 4$ , a three-point extrapolation becomes possible for  $N_{\max} \geq 8$ . Extrapolations are shown only in the  $\hbar\omega$  region safely above any crossing point for the ground state  $Q$  and  $r_p$ .) The extrapolations for  $Q$  [Fig. 3 (a)] and  $r_p$  [Fig. 3 (b)], for the Daejeon16 results, were seen in Part I to be remarkably robust, *i.e.*, independent of  $N_{\max}$  and  $\hbar\omega$ . The extrapolated values are also consistent with both experiment (squares) and the GFMC AV18+IL7 results [33] (crosses). However, for the harder JISP16 and LENPIC interactions, three-point exponential extrapolation yields results which are significantly less robust, and thus extrapolations for these interactions are not shown in Fig. 2 or 3 (but may be found in the Supplemental Material [46]).

We can again consider the results of a simple three-point exponential extrapolation for the  $B(E2)$  [Fig. 2 (d)]. For the two highest  $N_{\max}$  values, the extrapolations become largely consistent and  $\hbar\omega$  independent (over the  $\hbar\omega$  range shown), suggesting that extrapolation might be feasible. These extrapolations are also roughly consistent with experiment (square) and the GFMC AV18+IL7 result [33] (cross). Note that exponential extrapolation does not appear to be helpful for the ratio  $B(E2)/(eQ)^2$  [Fig. 2 (g)], not unexpectedly, since the small changes with  $N_{\max}$  would not appear, even by eye, to follow a simple exponential convergence pattern. Then, as noted above, the convergence of  $B(E2)/(e^2r_p^4)$  is less exponential, as indicated by  $\eta$  [Fig. 4 (right)], than for the  $B(E2)$  itself. Indeed, simple three-point exponential extrapolation [Fig. 2(j)] does not yield a consistent value.

### III. $E2$ TRANSITION STRENGTHS BY CALIBRATION TO THE GROUND STATE RADIUS IN $p$ -SHELL NUCLEI

#### A. Overview of results

We turn now to transitions in nuclides where the ground state angular momentum does not support a quadrupole moment [Fig. 1 (solid circles)]. We consider transitions from the first excited state to the ground state — or, more generally, from the first excited state for which an  $E2$  transition is allowed, by angular momentum and parity selection rules, to the ground state: namely,  $2^+ \rightarrow 0^+$  transitions in the mirror nuclides  $^{10}\text{Be}$  and  $^{10}\text{C}$  (Sec. III B) and in  $^{12}\text{C}$  (Sec. III C), the  $5/2^+ \rightarrow 1/2^+$

transition in  $^{11}\text{Be}$  (Sec. III D), and  $3/2^- \rightarrow 1/2^-$  transitions in the mirror nuclides  $^{13}\text{C}$  and  $^{13}\text{N}$  (Sec. III E). The  $E2$  strengths [15, 24, 47] are known except in  $^{11}\text{Be}$  and  $^{13}\text{N}$ , while the radii [19] are known except in  $^{10}\text{C}$  and  $^{13}\text{N}$  (Fig. 1). For  $^{10}\text{Be}$ , where the strength of the transition from the second excited  $2^+$  state to the ground state is also experimentally known [49], we consider this transition as well (Sec. III B), and, for  $^{12}\text{C}$ , where the quadrupole moment of the excited  $2^+$  state is experimentally known [30, 31], we consider this quadrupole moment in relation to the ground state radius (Sec. III C). We also make note of the calculated dimensionless ratio  $B(E2)/(eQ)^2$ , involving the excited state quadrupole moment, for these various transitions, as a diagnostic of axially symmetric rotational structure and thus of the relevance of  $B(E2)/(e^2r_p^4)$  to the deformation, to which we return in Sec. IV.

For a concise overview of the *ab initio* results for  $B(E2)/(e^2r_p^4)$ , in Fig. 5, we restrict our attention to a single, fixed value for the oscillator parameter  $\hbar\omega$ , namely,  $\hbar\omega = 20$  MeV (as in Figs. 4 and 5 of Part I), and examine the  $N_{\max}$  dependence of the calculated results. The results of three-point exponential extrapolation (small circles) are again indicated in the case of the Daejeon16 interaction. The experimental results are shown where available (horizontal lines, with error bands), and GFMC AV18+IL7 predictions [33] (crosses) are shown for the  $A = 10$  nuclides [4, 48]. Comprehensive plots of the calculated (and extrapolated) observables and ratios, as functions of both  $N_{\max}$  and  $\hbar\omega$ , for both proton and neutron observables, are provided in the Supplemental Material [46], along with numerical tabulations of the calculated observables.

#### B. $^{10}\text{Be}$ & $^{10}\text{C}$

Comparing the  $A = 10$  mirror nuclei, we may note that the convergence of  $B(E2)/(e^2r_p^4)$  is considerably slower for the proton-rich  $^{10}\text{C}$  [Fig. 5(b)] than for the neutron-rich  $^{10}\text{Be}$  [Fig. 5(a)]. Relative differences are about twice as large between the values for successive  $N_{\max}$  at the highest  $N_{\max}$  shown, but with similar difference ratios ( $\eta \approx 0.8$ ) for both nuclei.

The presumed  $\alpha + \alpha + 2n$  cluster molecular structure of the  $^{10}\text{Be}$  ground state (*e.g.*, Refs. [50–54]), together with the corresponding  $\alpha + \alpha + 2p$  structure of the  $^{10}\text{C}$  mirror nucleus, provides an ostensible explanation for the difference in convergence rates. The  $E2$  operator is only sensitive to the protons. In this picture, the protons in  $^{10}\text{Be}$  are all localized within the  $\alpha$  clusters, while, in  $^{10}\text{C}$ , two of the protons are in more diffuse molecular orbitals, which are more difficult to describe in an oscillator basis.

In  $^{10}\text{Be}$ , both the first and second  $2^+$  states are bound, lying below the neutron breakup threshold [22]. If one were to assume a simple, axially symmetric rotational picture, the  $2_1^+$  state (at 3.4 MeV) would be a member of the ground-state  $K = 0$  rotational band, while the  $2_2^+$



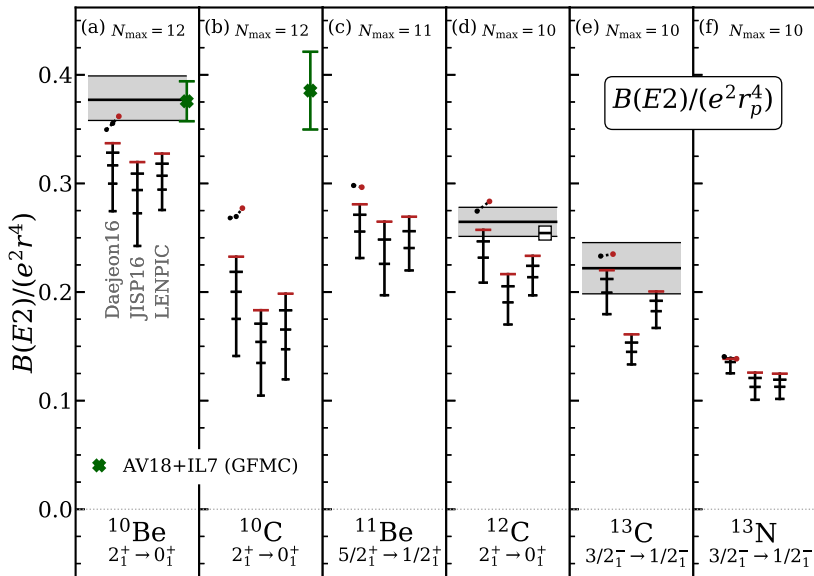


FIG. 5. Calculated ratios  $B(E2)/(e^2 r_p^4)$ , for transitions involving the ground states of nuclides in the  $p$  shell, considering cases in which the ground-state angular momentum does *not* support a quadrupole moment, namely,  $^{10}\text{Be}$ ,  $^{10}\text{C}$ ,  $^{11}\text{Be}$ ,  $^{12}\text{C}$ ,  $^{13}\text{C}$ , and  $^{13}\text{N}$  (left to right). Results are obtained with the Daejeon16, JISP16, and LENPIC interactions (from left to right, within each panel). Exponential extrapolations for  $B(E2)/(e^2 r_p^4)$  (small circles, dotted lines) are provided, for the Daejeon16 results only (plotted with  $N_{\text{max}}$  increasing from left to right). For comparison, the experimental ratios [19, 24, 47] are shown (horizontal line and error band), as are the GFM AV18+IL7 predictions [4, 48] for  $A = 10$  (crosses). For  $^{12}\text{C}$ , the ratio deduced from the more recent  $B(E2)$  measurement of D’Alessio *et al.* [15] is also included (horizontal line and error band, shown as narrow open box).

state (at 6.0 MeV) would be understood to be the band head of a low-lying  $K = 2$  side band [see Fig. 1(a) of Ref. [55]]. However, the existence of a low-lying  $K = 2$  band is suggestive of triaxial structure [51, 53, 55, 56], which implies  $K$  mixing [57]. The  $2_1^+ \rightarrow 0_1^+$  strength is known from Doppler-shift lifetime measurements [49, 58, 59], which give  $B(E2; 2_1^+ \rightarrow 0_1^+) = 9.34({}_{-36}^{+46}) e^2 \text{fm}^4$  [47]. For the  $2_2^+ \rightarrow 0_1^+$  transition, the  $2_2^+$  lifetime is newly measured by McCutchan *et al.* [49], since the most recent evaluation [22], giving  $B(E2; 2_2^+ \rightarrow 0_1^+) = 0.11(2) e^2 \text{fm}^4$ . We consider convergence of both the  $2_1^+ \rightarrow 0_1^+$  and  $2_2^+ \rightarrow 0_1^+$  transitions, and the relevant dimensionless ratios, in calculations with the Daejeon16 interaction, in Fig. 6.<sup>2</sup>

From GFMC calculations [49], it has been observed that these two  $2^+$  states are subject to mixing, and that their energy separation, and thus the actual degree of mixing, is highly sensitive to the details of the internucleon interaction. The calculated  $E2$  strengths may then be expected to be sensitive to such mixing. In NCCI calculations, even for a given interaction, the mixing is furthermore sensitive to the convergence of the energy separation of the calculated levels (and thus the energy denominator for mixing). Calculations with the Daejeon16 interaction give rapidly converging excitation en-

ergies for both these  $2^+$  states, as shown in Fig. 6(a), especially for the  $2_1^+$  state, mitigating such concerns. These predicted excitation energies also agree with experiment (solid squares) to well within half an MeV. However, in calculations with the harder JISP16 and LENPIC interactions, the  $2_2^+$  excitation energy is still poorly converged, and therefore so is the separation in the  $2^+$  energies.

The NCCI calculated  $E2$  strength for the  $2_1^+ \rightarrow 0_1^+$  transition [Fig. 6(c)] shows some hints of shouldering, as well as a crossing point for curves of successive  $N_{\text{max}}$  at  $\hbar\omega \approx 11 \text{ MeV} - 12 \text{ MeV}$ , in the general vicinity of the experimental value. Taking the dimensionless ratio  $B(E2)/(e^2 r_p^4)$  [Fig. 6(e)] eliminates much of the  $\hbar\omega$  dependence, and somewhat tames the  $N_{\text{max}}$  dependence. The ratio converges steadily from below, much as seen above for  $^9\text{Be}$  [Fig. 2(j)], approaching both the experimental ratio (solid square) and the GFMC AV18+IL7 prediction [4, 48] (cross). An exponential extrapolation for the ratio involving  $B(E2; 2_1^+ \rightarrow 0_1^+)$  [Fig. 6(e) (dotted curves)] would place the Daejeon16 prediction above the last calculated result ( $\approx 0.35$ ) by somewhere between once and twice again the size of last “step”, and thus generally within the experimental uncertainties. (Calibrating to the experimental ground state point-proton radius gives the scale shown at right.)

The dimensionless ratios, and thus estimated  $B(E2)$ , obtained with the JISP16 and LENPIC interactions [returning to Fig. 5(a)] might superficially appear to behave similarly to those for Daejeon16, but on closer examina-

<sup>2</sup> Results for the  $2_1^+$  excitation energy and  $2_1^+ \rightarrow 0_1^+$   $E2$  strength, with the Daejeon16 interaction, were previously shown in Fig. 2 of Ref. [55].

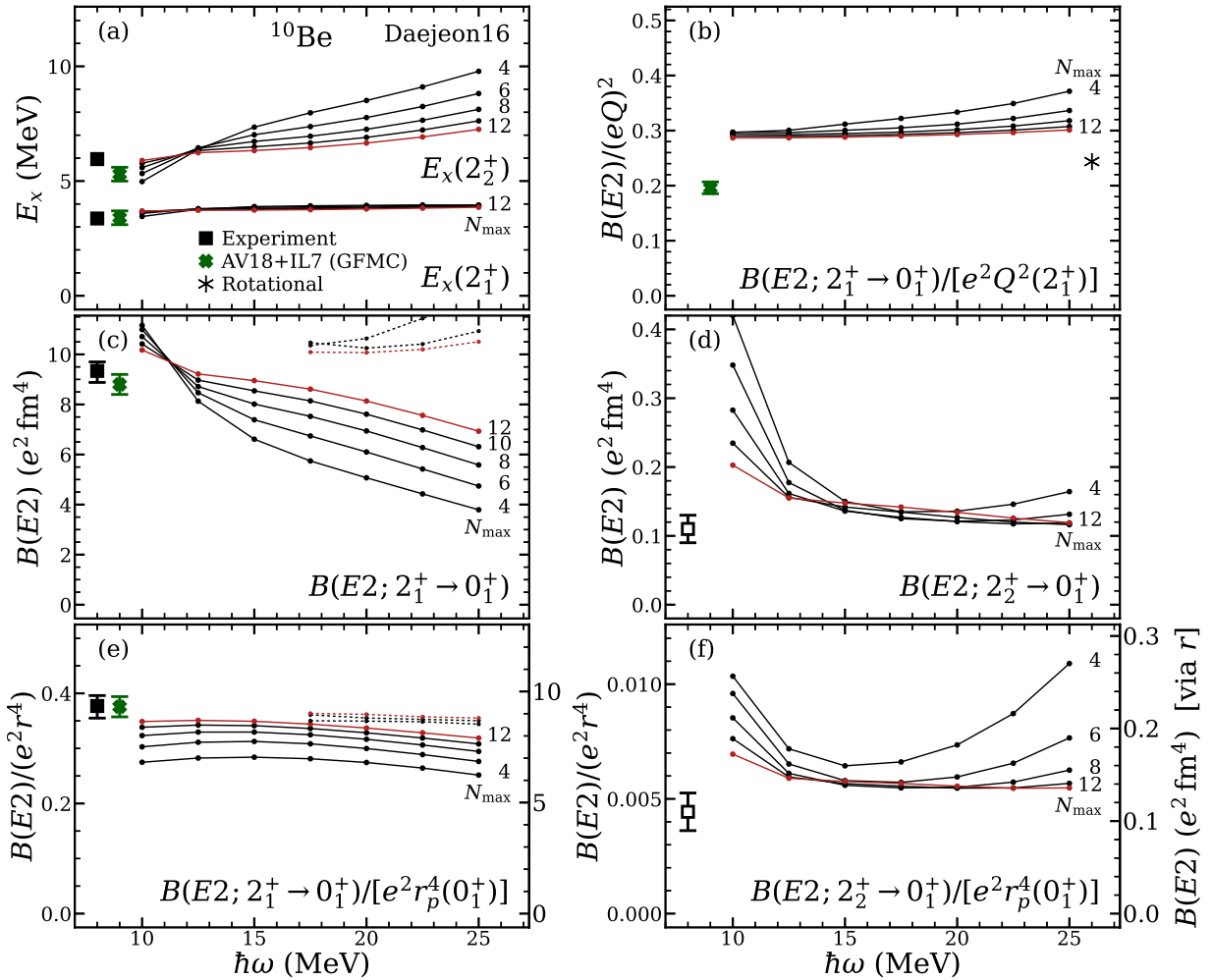


FIG. 6. Calculated observables for  $^{10}\text{Be}$ : (a) the  $2_1^+$  and  $2_2^+$  excitation energies, (b) the dimensionless ratio  $B(E2)/(eQ)^2$ , for the transition from the  $2_1^+$  state and taken relative to the quadrupole moment of that state, (c,d) the  $E2$  strengths  $B(E2; 2_1^+ \rightarrow 0_1^+)$  and  $B(E2; 2_2^+ \rightarrow 0_1^+)$ , and (e,f) the corresponding dimensionless ratios  $B(E2)/(e^2 r_p^4)$ , taken relative to the ground state radius. Calculated values, for the Daejeon16 interaction, are shown as functions of the basis parameter  $\hbar\omega$ , for successive even values of  $N_{\max}$ , from  $N_{\max} = 4$  to 12 (as labeled). When calibrated to the experimentally deduced value for  $r_p$ , the ratio provides a prediction for the absolute  $B(E2)$  (scale at right). Exponential extrapolations (small circles, dotted lines) are provided, for selected observables. For comparison, the experimental values [19, 22, 47], including evaluated results (solid squares) and the recent first measurement of McCutchan *et al.* [49] for the  $2_2^+ \rightarrow 0_1^+$  strength (open squares), GFMCAV18+IL7 predictions [4, 48] (crosses) [off-scale in (d) and (f)], and the rotational  $E2$  ratio (asterisk) are shown.

tion the LENPIC results do not clearly show a geometric progression towards convergence. Although the calculated values at  $N_{\max} = 12$  differ by  $\lesssim 5\%$ , at this scale, the differences in calculated values across these different interactions cannot be distinguished from the effects of incomplete convergence.

For the  $2_2^+ \rightarrow 0_1^+$  transition, the NCCI calculated  $B(E2)$  [Fig. 6(c)] has a more dramatic  $\hbar\omega$ -dependence at low  $N_{\max}$ , but the curves rapidly flatten for higher  $\hbar\omega$ . In a rotational picture, this transition is an interband transition, and its strength might be expected to be strongly influenced by any small admixed contribution from the ground state band's in-band  $2 \rightarrow 0$  strength entering into the interband strength, due to mixing of the

two  $2^+$  states.

Such dependence on mixing effects is not the type of systematic convergence behavior which we might hope to offset by normalization to the radius. Indeed, taking the dimensionless ratio [Fig. 6(f)] does not yield any marked qualitative difference in the convergence pattern. Nevertheless, taking the ratio would appear (perhaps fortuitously) to provide some improvement in the convergence behavior. While increasing the spread of the curves for low  $N_{\max}$  ( $N_{\max} \lesssim 6$ ), it flattens and compresses the curves obtained at higher  $N_{\max}$ . We may thus read off an estimated ratio  $B(E2)/(e^2 r_p^4) \approx 0.006$ , or  $B(E2; 2_2^+ \rightarrow 0_1^+) \approx 0.14 e^2 \text{fm}^4$  (scale at right). The predicted interband transition strength is roughly consistent



with experiment (open square), although just outside the experimental uncertainties. This agreement in scale is notable given that the  $2_2^+ \rightarrow 0_1^+$  interband transition is so comparatively weak: nearly two orders of magnitude weaker than the collective in-band  $2_1^+ \rightarrow 0_1^+$  strength, and an order of magnitude weaker than the Weisskopf estimate for a typical single-particle strength in these nuclei ( $\approx 1.3 e^2 \text{fm}^4$ ).

For the strong, in-band  $2_1^+ \rightarrow 0_1^+$  transition [Fig. 6(c)] the GFMC AV18+IL7 prediction [4, 48, 49] (cross) is consistent with experiment, and in close agreement with the present prediction for the dimensionless ratio [Fig. 6(e)]. However, the GFMC AV18+IL7 prediction for the weaker interband transition, at  $1.7(1) e^2 \text{fm}^4$ , lies off scale in Fig. 6(d), as does the corresponding ratio in Fig. 6(f). Such a large difference in the calculated strength of the weaker transition is perhaps not surprising, given the large variations in mixing in the GFMC calculations [49].

If we consider the quadrupole moment of the  $2_1^+$  state in relation to the  $2_1^+ \rightarrow 0_1^+$  transition strength, the rotational model (with  $K = 0$ ) gives  $B(E2)/(eQ)^2 = 49/(64\pi) \approx 0.2437$ . In the calculations with with Daejeon16 interaction, shown in Fig. 6(b),<sup>3</sup> this ratio appears to be well converged, but to a value  $\approx 20\%$  higher than the rotational value.<sup>4</sup> Given the above discussion of mixing and triaxiality, we should perhaps not be surprised if the calculated  $2^+$  states are mixed relative to the pure rotational  $K = 0$  and 2 states, leading to a breakdown of the axially symmetric rotational picture.

### C. $^{12}\text{C}$

Moving on to  $^{12}\text{C}$ , the  $2_1^+$  state (at 4.4 MeV) lies below the  $\alpha$  breakup threshold [20] and is interpreted as a member of the  $K = 0$  ground-state band. We consider the  $2_1^+ \rightarrow 0_1^+$  transition [Fig. 5(d)]. The ratios  $B(E2)/(e^2 r_p^4)$  calculated with the JISP16 and LENPIC interactions, at  $N_{\text{max}} = 10$ , are  $\approx 10\text{--}20\%$  lower than obtained with the Daejeon16 interaction. Although the convergence rates appear to be roughly similar for these calculations, it is unclear how much of the difference in calculated values might still be due to differences in convergence, rather than differences in the true predictions with these interactions.

Let us examine the results of the calculations with the Daejeon16 interaction, in Fig. 7. The excitation energy [Fig. 7(a)] is seen to be well converged and consistent with experiment (solid square).

The NCCI calculated  $E2$  strength [Fig. 7(c)], again, shows some hints of shouldering and a crossing point (at  $\hbar\omega \approx 11 \text{ MeV} \text{--} 12 \text{ MeV}$ ), and these features are in the general vicinity of the experimental strength. In particular, the evaluated  $E2$  strength is  $B(E2; 2_1^+ \rightarrow 0_1^+) = 7.9(4) e^2 \text{fm}^4$  [47] (solid square), while the more recent electron scattering experiment of D'Alessio *et al.* [15] yields a consistent result, but with smaller uncertainties, of  $B(E2; 2_1^+ \rightarrow 0_1^+) = 7.63(19) e^2 \text{fm}^4$  (open square). The results of an exponential extrapolation (dotted curves) seem to be tending higher than experiment, at  $\approx 9 e^2 \text{fm}^4$ , but not robustly.

Taking the dimensionless ratio  $B(E2)/(e^2 r_p^4)$  [Fig. 7(d)] once again eliminates much of the  $\hbar\omega$  dependence, while also modestly improving the  $N_{\text{max}}$  dependence, thereby permitting a more concrete comparison to be made. The calculated ratios are consistent in scale with the experimental results. However, if we take the evaluated  $B(E2)$  (solid square), they are on track to exceed the upper end of the experimental uncertainties, and, if we take D'Alessio *et al.* result (open square), they already lie above the experimental uncertainties, by  $N_{\text{max}} = 10$ , in the vicinity of  $\hbar\omega = 15 \text{ MeV}$ . The exponential extrapolations (dotted curves) remove most of the remaining  $\hbar\omega$  dependence but are still creeping upwards with increasing  $N_{\text{max}}$ . Estimating  $B(E2)/(e^2 r_p^4) \approx 0.28\text{--}0.30$ , gives an estimated  $B(E2)$  similarly tending above experiment, namely,  $\approx 8\text{--}9 e^2 \text{fm}^4$  (scale at right).

Both in the context of rotational structure and for comparison with experiment, it is of interest here to mention the quadrupole moment of the  $2^+$  state [Fig. 7(e)]. The quadrupole moment is experimentally known, but with large uncertainties, from the reorientation effect in Coulomb excitation [30]. The evaluated experimental quadrupole moment is  $Q(2_1^+) = +6(3) \text{ fm}^2$  [18] (solid square). However, the more recent experiment of Saiz-Lomas *et al.* [31] gives  $Q(2_1^+) = +9.3(_{-38}^{+35}) \text{ fm}^2$  (open square). While the uncertainties overlap with the prior evaluated moment, the central value from the new measurement is much larger.

The calculated ratio  $B(E2; 2_1^+ \rightarrow 0_1^+)/[eQ(2^+)]^2$  [Fig. 7(b)]<sup>5</sup> closely matches the rotational prediction  $B(E2; 2 \rightarrow 0)/[eQ(2)]^2 = 49/(64\pi) \approx 0.24$  (asterisk). Calci and Roth also verified this correlation, for a variety of NCCI calculations, in Fig. 4 of Ref. [8] (see also Fig. 6 of Ref. [15]). The experimental uncertainties on the evaluated quadrupole moment (solid square) leave the ratio  $B(E2)/(eQ)^2$  poorly constrained (although the central value, in fact, happens to be closely consistent with the rotational prediction). However, the more recent measurement (open square) is in strong tension with the rotational prediction, and thus with the present NCCI

<sup>3</sup> Calculations of  $B(E2)/(eQ)^2$  for  $^{10}\text{Be}$  and  $^{10}\text{C}$  with the Daejeon16 interaction, for  $N_{\text{max}} \leq 10$ , have previously been reported by Li *et al.* [17].

<sup>4</sup> Deviations from axially symmetric rotational relations within the nominal  $K = 0$  ground state band, for both proton and neutron  $E2$  matrix elements, may already be seen in Fig. 13(b) of Ref. [11], for calculations with the JISP16 interaction.

<sup>5</sup> Calculations of  $B(E2)/(eQ)^2$  for  $^{12}\text{C}$  with the Daejeon16 interaction have also previously been reported by Li *et al.* [17].

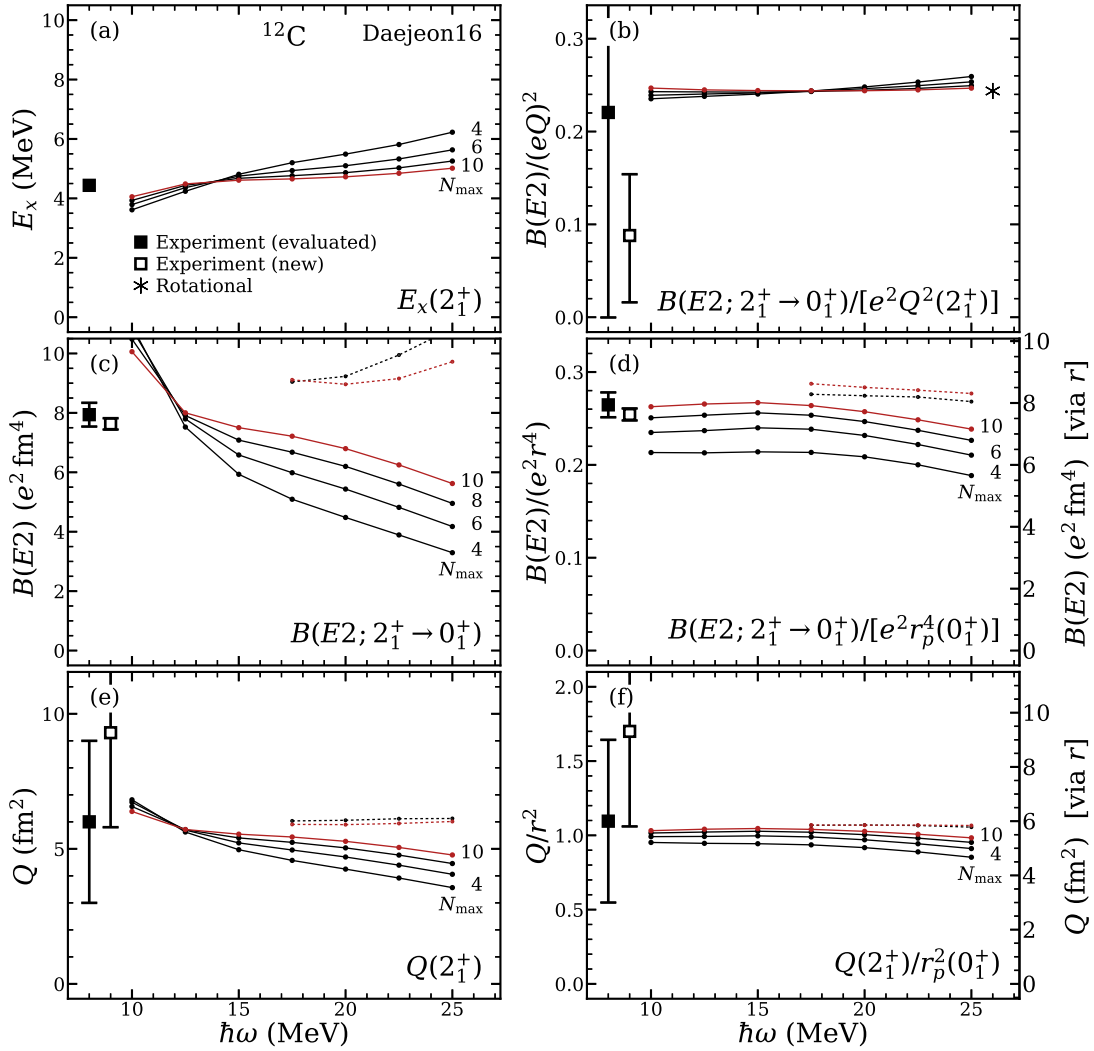


FIG. 7. Calculated observables for  $^{12}\text{C}$ : (left) (a) the  $2^+$  excitation energy, (c)  $B(E2; 2_1^+ \rightarrow 0_1^+)$ , and (e) the excited-state quadrupole moment  $Q(2_1^+)$ , and (right) dimensionless ratios constructed from these observables, including (b)  $B(E2)/(eQ)^2$ , (d)  $B(E2)/(e^2 r_p^4)$ , taken relative to the ground state proton radius, and (f)  $Q/r_p^2$ , again taken relative to the ground state radius. Calculated values, for the Daejeon16 interaction, are shown as functions of the basis parameter  $\hbar\omega$ , for successive even values of  $N_{\max}$ , from  $N_{\max} = 4$  to 10 (as labeled). When calibrated to the experimentally deduced value for  $r_p$ , the ratios provides predictions for the absolute  $B(E2)$  and  $Q$  (scale at right). Exponential extrapolations (small circles, dotted lines) are provided, for selected observables. For comparison, the experimental values [19, 20] are shown, taking either the evaluated  $B(E2)$  [47] and  $Q$  [18] (solid squares) or the more recent measurements of D’Alessio *et al.* [15] and Saiz-Lomas *et al.* [31], respectively, for these observables (open squares), and the rotational  $E2$  ratio (asterisk) is also shown.

predictions as well. (See also Fig. 1 of Ref. [31], which highlights the conflict between the experimental result of that paper and various *ab initio* and model predictions.)

The calculated dimensionless ratio  $Q/r_p^2$  [Fig. 7(f)], involving the excited state quadrupole moment but ground state radius, which may be used to estimate the quadrupole moment by calibration to the ground state radius, has little freedom to surprise us in its convergence behavior, given that we have already examined  $B(E2)/(e^2 r_p^4)$  [Fig. 7(b)]. That is to say, since we have found the calculated  $B(E2)/(eQ)^2$  [Fig. 7(d)] to be essentially constant, the calculated  $Q/r_p^2$  must be simply proportional to the square root of the calculated

$B(E2)/(e^2 r_p^4)$  [Fig. 7(d)], so that the overall behavior is the same, but with all relative differences approximately halved. Normalizing to the experimentally deduced  $r_p = 2.340(3)$  fm [19] (scale at right) allows us to estimate  $Q(2_1^+) \approx 6.0$  fm $^2$ . This finding is robust across choice of interaction (see Fig. 3 of Ref. [32]). Here, again, if we take the evaluated experimental quadrupole moment (solid square), the predictions are near the central value, but, if we take the new measurement [31] (open square), the predictions are at the lower edge of the uncertainties.

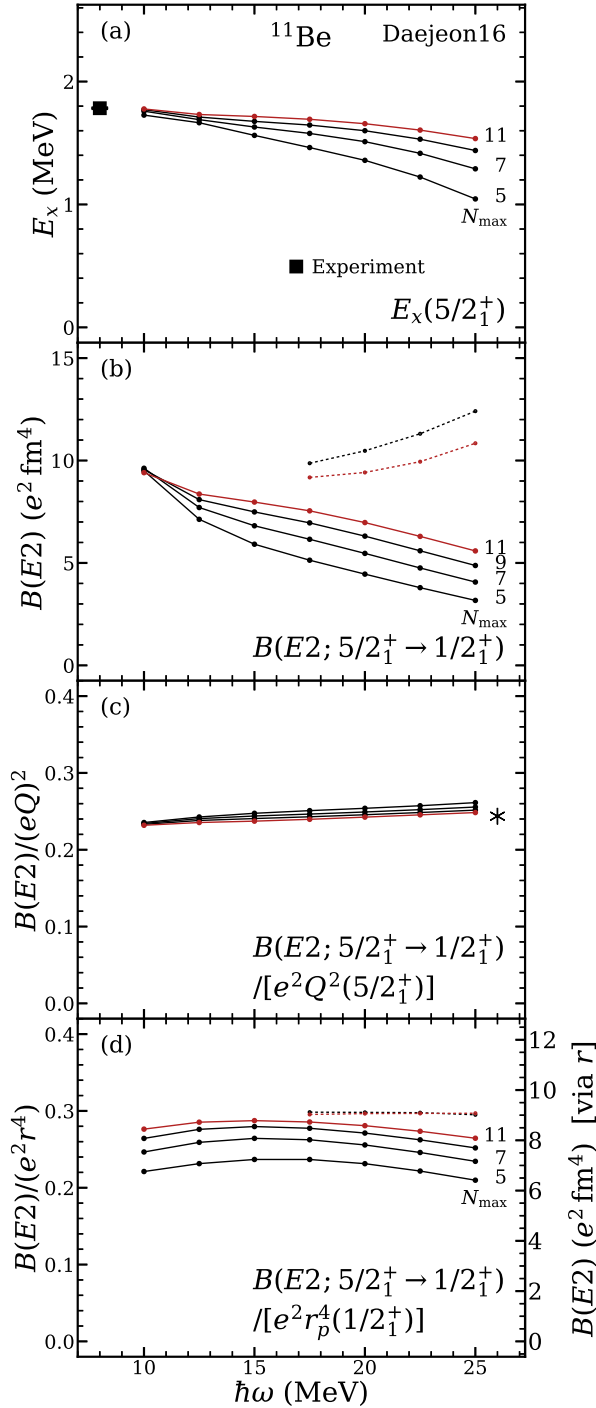
D.  $^{11}\text{Be}$ 

FIG. 8. Calculated observables for  $^{11}\text{Be}$ : (a) the  $5/2_1^+$  excitation energy, (b)  $B(E2; 5/2_1^+ \rightarrow 1/2_1^+)$ , (c) the dimensionless ratio  $B(E2)/(eQ)^2$ , taken relative to the excited  $5/2_1^+$  state quadrupole moment, (d) the dimensionless ratio  $B(E2)/(e^2r_p^4)$ , taken relative to the ground state radius. Calculated values, for the Daejeon16 interaction, are shown as functions of the basis parameter  $\hbar\omega$ , for successive even values of  $N_{\max}$ , from  $N_{\max} = 5$  to 11 (as labeled). When calibrated to the experimentally deduced value for  $r_p$ , the ratio provides a prediction for the absolute  $B(E2)$  (scale at right). Exponential extrapolations (small circles, dotted lines) are provided, for selected observables. For comparison, the experimental excitation energy [23] (square) is also shown.

For  $^{11}\text{Be}$ , we consider the  $5/2^+ \rightarrow 1/2^+$  transition [Fig. 5(c)]. The  $1/2^+$  ground state [23] is of non-normal parity [60], *i.e.*, opposite to that expected from simple sequential filling of harmonic oscillator shells. The  $5/2^+$  state (at 1.8 MeV), which lies above the neutron breakup threshold and has a width of  $\approx 100$  keV, is the first excited state of the same parity [23]. The convergence patterns, for all three interactions, are qualitatively similar to those seen above for neighboring  $^{10}\text{Be}$  [Fig. 5(a)]. Any apparent differences in calculated values across the three interactions, at finite  $N_{\max}$ , could well simply reflect the clearly incomplete convergence.

A closer examination of the convergence obtained with the Daejeon16 interaction, in Fig. 8, shows that, while three-point exponential extrapolation is of little use for the  $B(E2)$  itself [Fig. 8(b)], it is particularly robust, that is, independent of  $N_{\max}$  and  $\hbar\omega$ , for the dimensionless ratio [Fig. 8(d)]. This is true at least for the limited range of calculations available (from calculations with  $N_{\max} \geq 5$ , a three-point extrapolation only becomes possible for  $N_{\max} \geq 9$ ).<sup>6</sup> Calibration to the experimentally deduced value of  $r_p$  gives the scale at right in Fig. 8(d). Combining an extrapolated  $B(E2)/(e^2r_p^4) \approx 0.30$ , for the Daejeon16 interaction, with the experimentally deduced  $r_p = 2.351(16)$  fm [19], gives an estimated  $B(E2; 5/2^+ \rightarrow 1/2^+) \approx 9.2 e^2\text{fm}^4$ .

Note that the  $5/2^+ \rightarrow 1/2^+$  transition, in a rotational picture, is interpreted as a  $K = 1/2$  in-band transition [see Fig. 2(b) of Ref. [36]]. (Coriolis energy staggering raises the  $3/2^+$  band member above the  $5/2^+$  band member.) The calculated  $B(E2)/(eQ)^2$  [Fig. 8(c)], involving the excited  $5/2^+$  state quadrupole moment, is relatively well converged and consistent with the rotational value  $B(E2)/(eQ)^2 = 49/(64\pi) \approx 0.2437$  for such a transition.<sup>7</sup>

E.  $^{13}\text{C}$  &  $^{13}\text{N}$ 

Finally, let us consider the  $3/2^- \rightarrow 1/2^-$  transitions in the  $A = 13$  mirror nuclei,  $^{13}\text{C}$  [Fig. 5(e)] and  $^{13}\text{N}$  [Fig. 5(f)]. In  $^{13}\text{C}$ , the  $3/2^-$  excited state is bound, while, in the mirror nuclide  $^{13}\text{N}$ , this excited state lies above the proton breakup threshold, and has a width of  $\approx 64$  keV [24].

The convergence rates for  $B(E2)/(e^2r_p^4)$  are generally similar in these two cases. However, the convergence is

<sup>6</sup> States of non-normal parity are obtained from oscillator configurations with an odd number of oscillator excitations relative to the lowest Pauli-allowed filling of oscillator shells, and thus in odd- $N_{\max}$  NCCI spaces.

<sup>7</sup> Rough consistency with the axially symmetric rotational relations within a  $K = 3/2$  band may already be seen for this transition in Fig. 11(b) of Ref. [11], for calculations with the JISP16 interaction.

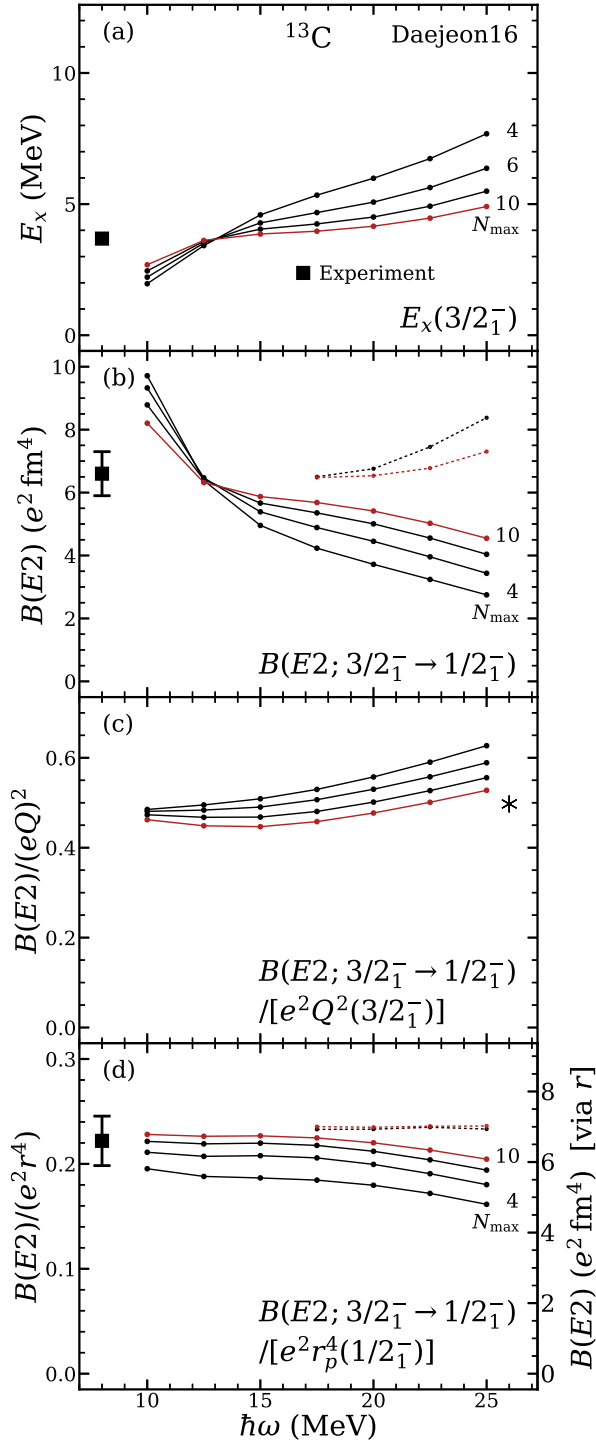


FIG. 9. Calculated observables for  $^{13}\text{C}$ : (a) the  $3/2_1^-$  excitation energy, (b)  $B(E2; 3/2_1^- \rightarrow 1/2_1^-)$ , (c) the dimensionless ratio  $B(E2)/(eQ)^2$ , taken relative to the excited  $3/2_1^-$  state quadrupole moment, and (d) the dimensionless ratio  $B(E2)/(e^2 r_p^4)$ , taken relative to the ground state radius. Calculated values, for the Daejeon16 interaction, are shown as functions of the basis parameter  $\hbar\omega$ , for successive even values of  $N_{\max}$ , from  $N_{\max} = 4$  to 10 (as labeled). When calibrated to the experimentally deduced value for  $r_p$ , the ratio provides a prediction for the absolute  $B(E2)$  (scale at right). Exponential extrapolations (small circles, dotted lines) are provided, for selected observables. For comparison, experimental values [19, 24] (squares) are also shown.

less smooth for  $^{13}\text{N}$ , at least for the Daejeon16 calculations, where the values at higher  $N_{\max}$  become compressed (in fact, the value obtained for  $N_{\max} = 10$  lies marginally *below* that for  $N_{\max} = 8$ ). The calculated ratios, at finite  $N_{\max}$ , are higher for  $^{13}\text{C}$  than for  $^{13}\text{N}$ , but, again, different convergence rates can render such naive comparison misleading.

The convergence of the Daejeon16 results for  $^{13}\text{C}$  is shown in more detail in Fig. 9. The excitation energy for the  $3/2_1^-$  state [Fig. 9(a)] is consistent with experiment. The calculated  $B(E2)$  values [Fig. 9(b)] are on the same scale as experiment [24], and are plausibly consistent (*e.g.*, from the crossing points of the curves or taking the exponential extrapolations as a crude guide), but cannot be compared quantitatively.

Turning to the ratio  $B(E2)/(e^2 r_p^4)$  [Fig. 9(d)], the calculated values are relatively flat with respect to  $\hbar\omega$ , and the spacing is decreasing rapidly with  $N_{\max}$  ( $\eta \approx 0.6$  at  $\hbar\omega = 20$  MeV). The extrapolations obtained at  $N_{\max} = 8$  and  $N_{\max} = 10$  are nearly indistinguishable and independent of  $\hbar\omega$ , suggesting a ratio of  $B(E2)/(e^2 r_p^4) \approx 0.23$ – $0.24$ . This lies just within the uncertainties of the experimental value  $B(E2)/(e^2 r_p^4) = 0.22(2)$  [19, 24].

Note that the  $3/2_1^- \rightarrow 1/2_1^-$  transition, in a rotational picture, is most simply interpreted as a  $K = 1/2$  in-band transition. The calculated  $B(E2)/(eQ)^2$  [Fig. 9(c)], involving the excited  $3/2_1^-$  state quadrupole moment, is not as well converged as in some of the previous examples, but is roughly consistent with the rotational value  $B(E2)/(eQ)^2 = 25/(16\pi) \approx 0.4947$  for such a transition.

#### IV. DEFORMATION

Finally, let us explore what the ratios of the form  $B(E2)/(e^2 r^4)$  indicate for the nuclear quadrupole deformation, via the rotational relation given in (14) of Part I. That is, for the proton observables,

$$\frac{B(E2; J_i \rightarrow J_f)}{Z^2 e^2 r_p^4} = \left(\frac{5}{4\pi}\right)^2 (J_i K 20 | J_f K)^2 \beta_p^2,$$

where  $K$  is the angular momentum projection of the rotational intrinsic state along the symmetry axis (see Sec. II.3 of Part I). The analogous ratio  $B(E2_n)/(e^2 r_n^4)$ , *i.e.*, calculated using the neutron quadrupole operator and neutron radius, similarly yields the neutron deformation  $\beta_n$ , with the replacement of  $Z$  by  $N$  in the above expression. The resulting deformations thus extracted from the transitions considered in this work are shown in Fig. 10, for both the protons (top) and neutrons (bottom).

Here it is worth highlighting that the traditional expression commonly used to extract the nuclear deformation from the  $0^+ \rightarrow 2^+$   $E2$  strength in empirical tabulations for even-even nuclei [47, 61], reproduced in (16) of

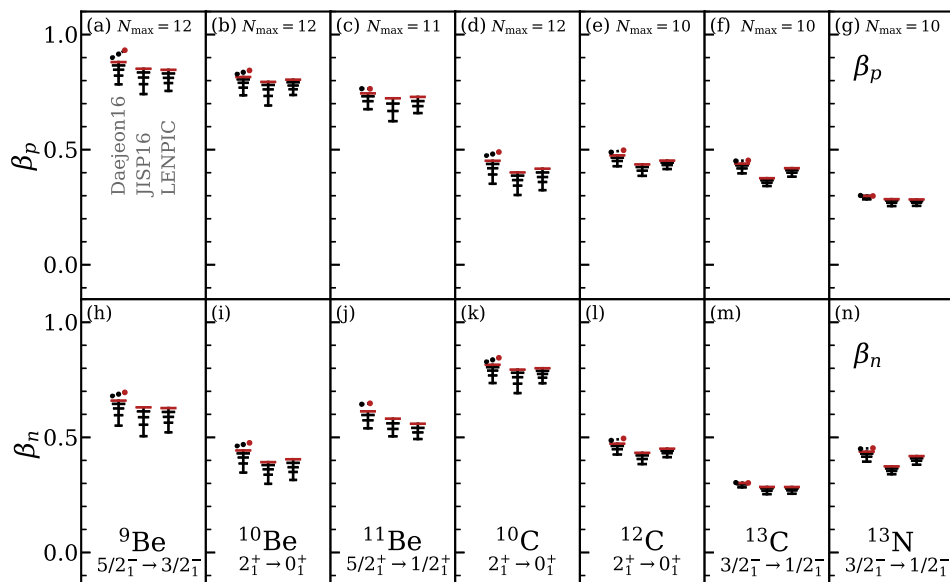


FIG. 10. Calculated proton (top) and neutron (bottom) deformations, as deduced from the ratios of the form  $B(E2)/(e^2r^4)$ , under the assumption of axially symmetric rotation, for the nuclides considered in this work. Results are obtained with the Daejeon16, JISP16, and LENPIC interactions (from left to right, within each panel). Calculated values are shown at fixed  $\hbar\omega = 20$  MeV and varying  $N_{\max}$  (increasing tick size), from  $N_{\max} = 4$  (or 5) to the maximum value indicated (at top). The initial and final states for the transition used are indicated (at bottom), with  $K$  as noted in the text.

Part I, namely,

$$\beta = \frac{4\pi}{3} \frac{B(E2; 0 \rightarrow 2)^{1/2}}{Zer_0^2 A^{2/3}},$$

is deduced from this same relation, but relies upon the textbook global phenomenological estimate for the radius ( $r \propto A^{1/3}$ ). This leads to notable discrepancies for the nuclei being considered here. For  $^{10}\text{Be}$ , the proton radius deduced from the measured charge radius [19] (see Sec. II.2 of Part I) is  $\approx 11\%$  higher than the global phenomenological estimate, or, for  $^{12}\text{C}$ ,  $\approx 10\%$  higher. This radius then enters quadratically into the determination of the  $\beta$ , doubling the effect (to  $\approx 20\%$ ). Thus, while the calculated  $B(E2)/(e^2r_p^4)$  is in general agreement with experiment for  $^{10}\text{Be}$  [Fig. 5(a)] and  $^{12}\text{C}$  [Fig. 5(d)], and thus the deduced (proton) deformations in Fig. 10(b,e) are in similar agreement with those deduced from the experimental ratio, the tabulated empirical deformations obtained from the very same measured  $E2$  strengths [47], but relying upon the global empirical fit estimate for the radius, are higher:  $\beta \approx 1.07$  for  $^{10}\text{Be}$  [Fig. 10(b)] and  $\beta \approx 0.58$  for  $^{12}\text{C}$  [Fig. 10(e)]. The tabulated deformation of  $\beta \approx 0.70$  for  $^{10}\text{C}$  [Fig. 10(d)] is likewise higher than calculated, but here the experimental charge radius is not known [19] to permit comparison with the experimental ratio.

We may also note that mirror symmetry holds to a very good approximation for the calculated ratios  $B(E2)/(e^2r^4)$ , and thus for the extracted deformations in Fig. 10, even though the *ab initio* calculations allow for isospin symmetry breaking (through the

Coulomb interaction between protons in the Daejeon16 and JISP16 calculations and through additional isospin symmetry breaking contributions to the nuclear force in the LENPIC calculations). In particular, the extracted deformations for the mirror nuclei  $^{10}\text{Be}$  [Fig. 10(b,i)] and  $^{10}\text{C}$  [Fig. 10(d,k)] are nearly indistinguishable, under interchange of the proton and neutron deformations, and similarly for  $^{13}\text{C}$  [Fig. 10(f,m)] and  $^{13}\text{N}$  [Fig. 10(g,n)]. Likewise, the calculated proton and neutron deformations for the  $N = Z$  nuclide  $^{12}\text{C}$  [Fig. 10(e,l)] are nearly indistinguishable.

For the Be isotopes, in the cluster molecular orbital interpretation [62–67], supported by microscopic antisymmetrized molecular dynamics (AMD) [53, 68, 69] and nuclear lattice effective field theory (NLEFT) calculations [70], as well as NCCI results [71], the nucleus consists of an underlying  $\alpha + \alpha$  dimer ( $^8\text{Be}$ ), with the additional “valence” neutrons occupying  $\pi$  (equatorial) or  $\sigma$  (polar) molecular orbitals. We might naively expect the proton deformation to be unchanged by the addition of spectator neutrons. However, even within the cluster molecular orbital description this cannot be taken as a given: the presence of the valence neutrons can affect the inter- $\alpha$  spacing, or perturb the structure of the  $\alpha$  particles, or induce recoil effects.<sup>8</sup> In the cluster molecular orbital picture, the valence neutron in the  $^9\text{Be}$  ground

<sup>8</sup> The proton and quadrupole and monopole operators entering into the definition of the deformation for this distribution (Sec. II.3 of Part I), are defined relative to the center of mass of the combined proton and neutron system [72]. The neutron

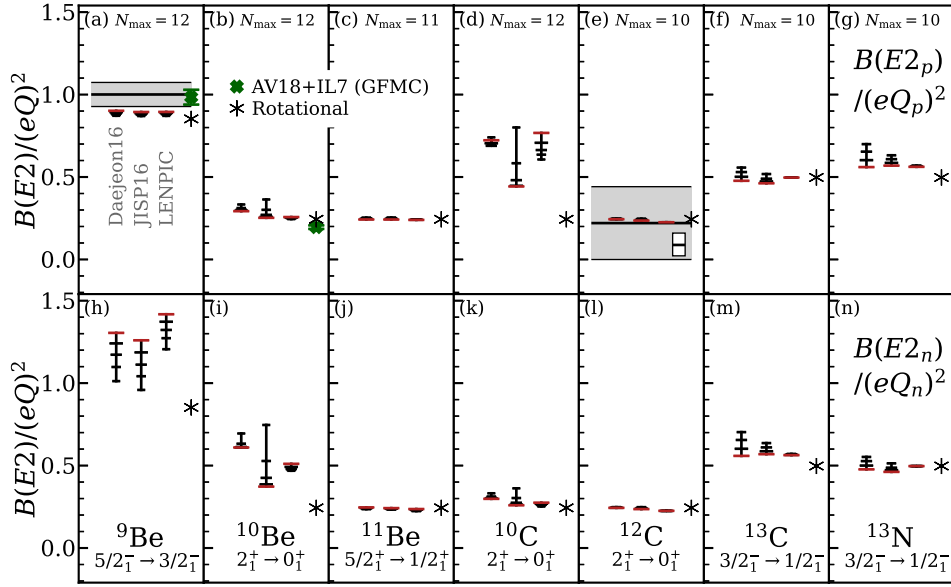


FIG. 11. Calculated ratios  $B(E2)/(eQ)^2$  obtained for the proton (top) and neutron (bottom) quadrupole operators, for the nuclides considered in this work. Results are obtained with the Daejeon16, JISP16, and LENPIC interactions (from left to right, within each panel). Calculated values are shown at fixed  $\hbar\omega = 20$  MeV and varying  $N_{\text{max}}$  (increasing tick size), from  $N_{\text{max}} = 4$  (or 5) to the maximum value indicated (at top). The initial and final states for the transition used are indicated (at bottom), with  $Q$  taken from the ground state for  ${}^9\text{Be}$  and excited state otherwise. For comparison, the experimental ratios [19, 24, 47] are shown (horizontal line and error band), as are the GFMCAV18+IL7 predictions [4, 33, 48] [off-scale for  ${}^{10}\text{C}$  in (d)] (crosses), and rotational  $E2$  ratios (asterisks). For  ${}^{12}\text{C}$ , the ratio deduced from the more recent measurements of D’Alessio *et al.* [15] and Saiz-Lomas *et al.* [31] is also included (horizontal line and error band, shown as narrow open box).

state occupies a  $\pi$  equatorial orbital, which would be expected to lead to a more spherical overall distribution for the neutrons than for the protons. For the  ${}^{10}\text{Be}$  ground state, both neutrons occupy  $\pi$  orbitals. The AMD results indicate their influence is to induce an oblate deformation for the neutrons, which aligns orthogonally to the prolate proton deformation, yielding an overall triaxial deformation. The positive parity (parity-inverted) ground state of  ${}^{11}\text{Be}$  then is obtained from a  $\pi^2\sigma$  configuration of neutrons.

If we take the extracted deformations for the Be isotopes in Fig. 10 at face value, the proton deformation  $\beta_p$  [Fig. 10(a,b,c)] is not strictly constant across the nuclides, but demonstrates a gentle downward drift from  ${}^9\text{Be}$  to  ${}^{11}\text{Be}$ , with the calculated values declining from  $\approx 0.8$ – $0.9$  to  $\approx 0.7$ – $0.8$ . (The same caveats regarding incomplete convergence as discussed for the underlying ratio in Sec. III apply here as well.) The neutron deformation  $\beta_n$  [Fig. 10(h,i,j)] is more markedly variable, first descending from  $\approx 0.6$ – $0.7$  to  $\approx 0.4$ – $0.5$ , then rising again to  $\approx 0.6$ .

However, it is important to keep in mind that (14) of Part I is based on the assumption both of a rigid intrinsic deformation and of axially symmetric rotational relations for  $E2$  matrix elements. The deformation extracted from an  $E2$  transition [via the ratio of the form  $B(E2)/(e^2r^4)$ , by (14) of Part I] or from a quadrupole moment [via the ratio of the form  $Q/r^2$ , by (13) of Part I] will be consistent only if  $B(E2)/(eQ)^2$  takes on its rotational value. We have already made preliminary comparisons of  $B(E2)/(eQ)^2$  to the rotational ratio for several of the transitions discussed above (Secs. II and III). A more comprehensive overview of  $B(E2)/(eQ)^2$ , for all three interactions considered, and for both proton (top) and neutron (bottom) quadrupole observables, is provided in Fig. 11.

Even for  ${}^9\text{Be}$ , where we saw in Sec. II that the proton  $B(E2)/(eQ)^2$  [Fig. 11(a)] is relatively well-converged and lies not far above the rotational ratio, the analogous ratio for the neutron observables [Fig. 11(h)], is egregiously unconverged. Furthermore, by  $N_{\text{max}} = 12$  (at  $\hbar\omega = 20$  MeV), it is a factor of  $\approx 1.5$  above the rotational ratio, and tending higher. Correspondingly, the extracted neutron deformations, at  $\beta_n \gtrsim 0.6$ , are tending higher than the value  $\beta_n \approx 0.5$  obtained from the ground state quadrupole moment (Fig. 10 of Part I) and, given the breakdown of the rotational picture, should not be taken to be meaningful. One may speculate that this poor convergence of the neutron ratio is due to the behavior of the last neutron, which is bound in the  $3/2^-$

coordinates enter implicitly into these observables through their effect on the center of mass, and the addition of neutrons can affect proton observables by perturbing the center of mass, in a so-called recoil effect. As a prominent example, the enhanced proton radius in the neutron halo nucleus  ${}^6\text{He}$  is understood to arise from such a recoil effect [73].



ground state, but unbound in the  $5/2^-$  initial state for the transition [22].

Then, recall from Sec. III B that  $^{10}\text{Be}$  exhibits blatant deviations from the rotational value for  $B(E2)/(eQ)^2$  [Fig. 11(b)], by  $\approx 20\%$ , for the Daejeon16 interaction, and is suspected of triaxial, rather than axially symmetric, structure. The results for  $B(E2)/(eQ)^2$ , for the JISP16 and LENPIC interactions, actually match the rotational prediction more closely. However, the corresponding neutron ratios [Fig. 11(i)] are slow to converge and highly dependent upon interaction, but they are generally well above with the rotational ratio, indeed, in the Daejeon16 results,  $\gtrsim 2.5$  times the rotational value. Thus, again for  $^{10}\text{Be}$ , the neutron deformation extracted by application of the rotational relations is not meaningful, nor, given the overall deviations from axially symmetric rotational structure, would we have confidence in the proton deformation thus extracted.

For  $^{11}\text{Be}$ , the  $5/2^+$  initial state for the  $5/2^+ \rightarrow 1/2^+$  transition is likewise unbound against neutron emission [23], as for  $^9\text{Be}$  above. Nonetheless, in this case the calculated  $B(E2)/(eQ)^2$  is well-converged both for the protons [Fig. 11(c)] and for the neutrons [Fig. 11(j)], and closely agrees with the rotational ratio, across all three interactions. Thus, among the Be isotopes considered here, only for  $^{11}\text{Be}$  would it seem reasonable to attach meaning to the deformations extracted in Fig. 10. Note the lower overall deformation for the neutrons [Fig. 10(j)] than for the protons [Fig. 10(c)], ostensibly attributable to the net result of adding equatorial ( $\pi$ ) and polar ( $\sigma$ ) valence neutrons.

Turning to the C isotopes,  $^{10}\text{C}$  [Fig. 10(d,k)] is the mirror nuclide to  $^{10}\text{Be}$ , so there are similarly deviations from axially symmetric rotation,<sup>9</sup> and it is again not meaningful to extract a deformation from the  $B(E2)$ . However, for  $^{12}\text{C}$ , recall from Sec. III C that  $B(E2)/(eQ)^2$  [Fig. 11(e,l)] is robustly rotational. For  $^{13}\text{C}$ , as noted in Sec. III E, this ratio is less well converged, but generally consistent with the rotational value, which we find across interactions for both the proton [Fig. 11(f)] and neutron [Fig. 11(m)] ratios.

Thus, we may attach some credence to the extracted deformations for  $^{12}\text{C}$  [Fig. 10(e,l)] and  $^{13}\text{C}$  [Fig. 10(f,m)]. The extracted proton deformations ( $\approx 0.4$ – $0.5$ ) are essentially indistinguishable across these two nuclei, while, going from  $^{12}\text{C}$  to  $^{13}\text{C}$ , the neutron deformation drops (from  $\approx 0.4$ – $0.5$ , the same as for the protons in  $^{12}\text{C}$ ) to  $\approx 0.3$ , consistently across the different interactions considered.

<sup>9</sup> Intriguingly, we may observe significant deviations from mirror symmetry in the calculated  $B(E2)/(eQ)^2$  for  $^{10}\text{Be}$  and  $^{10}\text{C}$ , under interchange of proton and neutron observables, if we compare Fig. 11(d) with Fig. 11(i).

## V. CONCLUSION

Although  $E2$  transition strengths are often poorly convergent in NCCI calculations, it is already known that correlations with other calculated observables [8, 16] can be exploited to extract meaningful predictions. It is most natural and obvious to make of use correlations among the  $E2$  observables themselves, *e.g.*, predicting an  $E2$  strength by calibration to a known ground state quadrupole moment, where such an approach is possible. However, we demonstrate that correlations between the calculated  $E2$  strengths and the ground state radius can also be exploited. In the previous article (Part I), we assessed correlations between the  $E2$  moment and the radius, through the dimensionless ratio  $Q/r_p^2$ . In the present article (Part II), we explored correlations between low-lying  $E2$  transition strengths and the radius, with the goal of using the dimensionless ratio  $B(E2)/(e^2r_p^4)$  to predict an  $E2$  strength by calibration to a known ground state radius.

Correlations between  $E2$  strengths and the radius are not found to be as robust as those involving only  $E2$  observables, as seen in direct comparisons of the dimensionless ratios  $B(E2)/(eQ)^2$  and  $B(E2)/(e^2r_p^4)$  for the same transitions (*e.g.*, Fig. 2). Nonetheless, calibration to the ground state radius in many cases provides at least a rough prediction where none might otherwise be available, as we demonstrate for several  $p$ -shell nuclei for which the ground state angular momentum does not admit a quadrupole moment (Fig. 5). Furthermore, *ab initio* calculations for  $B(E2)/(e^2r_p^4)$  provide an indirect measure of the predicted deformation for these nuclei, under the assumption of axially symmetric rotation.

It is worth noting some *a priori* limitations to an approach which relies upon robust prediction of correlations between and  $E2$  transition strength and a ground state property, whether the quadrupole moment or the radius. Such approaches are geared towards eliminating smoothly varying systematic truncation error, rather than sudden changes arising from level crossings and the consequent two-state mixing [26]. Thus, in particular, they are not immediately applicable to transitions between normal and intruder states, which arise primarily from such mixing (*e.g.*, Ref. [74]). Moreover, the convergence properties of normal and intruder states in NCCI calculations are notably different (*e.g.*, Ref. [36]), so predictions of  $E2$  properties of the intruder states themselves, or transitions among them, are not likely candidates for calibration to ground state properties.

Nonetheless, we demonstrate that normalizing an  $E2$  observable to the appropriate power of the radius, to yield a dimensionless ratio, tames the  $\hbar\omega$  dependence of the results and, to a less dramatic extent, the  $N_{\text{max}}$  dependence of the results. We have explored the properties of such dimensionless ratios and their predictive value, for transitions between low-lying states and the ground state, for nuclei across the  $p$  shell.

## ACKNOWLEDGMENTS

We thank James P. Vary, Ik Jae Shin, and Youngman Kim for sharing illuminating results on ratios of observables, Augusto O. Macchiavelli for valuable discussions, and Scott R. Carmichael, Johann Isaak, and Shwetha L. Vittal for comments on the manuscript. This material is based upon work supported by the U.S. Department of Energy, Office of Science, under Awards No. DE-FG02-

95ER40934, DE-AC02-06CH11357, and DE-SC0023495 (SciDAC5/NUCLEI). This research used resources of the National Energy Research Scientific Computing Center (NERSC), a DOE Office of Science User Facility supported by the Office of Science of the U.S. Department of Energy under Contract No. DE-AC02-05CH11231, using NERSC awards NP-ERCAP0020422, NP-ERCAP0023497, and NP-ERCAP0026449.

- 
- [1] M. Pervin, S. C. Pieper, and R. B. Wiringa, Quantum Monte Carlo calculations of electroweak transition matrix elements in  $A = 6, 7$  nuclei, *Phys. Rev. C* **76**, 064319 (2007).
- [2] S. K. Bogner, R. J. Furnstahl, P. Maris, R. J. Perry, A. Schwenk, and J. Vary, Convergence in the no-core shell model with low-momentum two-nucleon interactions, *Nucl. Phys. A* **801**, 21 (2008).
- [3] P. Maris and J. P. Vary, *Ab initio* nuclear structure calculations of  $p$ -shell nuclei with JISP16, *Int. J. Mod. Phys. E* **22**, 1330016 (2013).
- [4] J. Carlson, S. Gandolfi, F. Pederiva, S. C. Pieper, R. Schiavilla, K. E. Schmidt, and R. B. Wiringa, Quantum Monte Carlo methods for nuclear physics, *Rev. Mod. Phys.* **87**, 1067 (2015).
- [5] D. Odell, T. Papenbrock, and L. Platter, Infrared extrapolations of quadrupole moments and transitions, *Phys. Rev. C* **93**, 044331 (2016).
- [6] R. Roth and M. Petri, Electromagnetic properties of nuclei from first principles: A case for synergies between experiment and theory, *Philos. Trans. R. Soc. London A* **382**, 2023011902024 (2023).
- [7] B. R. Barrett, P. Navrátil, and J. P. Vary, *Ab initio* no core shell model, *Prog. Part. Nucl. Phys.* **69**, 131 (2013).
- [8] A. Calci and R. Roth, Sensitivities and correlations of nuclear structure observables emerging from chiral interactions, *Phys. Rev. C* **94**, 014322 (2016).
- [9] G. H. Sargsyan, K. D. Launey, M. T. Burkey, A. T. Galant, N. D. Scielzo, G. Savard, A. Mercenne, T. Dytrych, D. Langr, L. Varriano, B. Longfellow, T. Y. Hirsh, and J. P. Draayer, Impact of clustering on the  ${}^8\text{Li}$   $\beta$  decay and recoil form factors, *Phys. Rev. Lett.* **128**, 202503 (2022).
- [10] M. A. Caprio, P. Maris, and J. P. Vary, Emergence of rotational bands in *ab initio* no-core configuration interaction calculations of light nuclei, *Phys. Lett. B* **719**, 179 (2013).
- [11] P. Maris, M. A. Caprio, and J. P. Vary, Emergence of rotational bands in *ab initio* no-core configuration interaction calculations of the Be isotopes, *Phys. Rev. C* **91**, 014310 (2015); Erratum: Emergence of rotational bands in *ab initio* no-core configuration interaction calculations of the Be isotopes, *Phys. Rev. C* **99**, 029902(E) (2019).
- [12] S. L. Henderson, T. Ahn, M. A. Caprio, P. J. Fasano, A. Simon, W. Tan, P. O'Malley, J. Allen, D. W. Bardayan, D. Blankstein, B. Frentz, M. R. Hall, J. J. Kolata, A. E. McCoy, S. Moylan, C. S. Reingold, S. Y. Strauss, and R. O. Torres-Isea, First measurement of the  $B(E2; 3/2^- \rightarrow 1/2^-)$  transition strength in  ${}^7\text{Be}$ : Testing *ab initio* predictions for  $A = 7$  nuclei, *Phys. Rev. C* **99**, 064320 (2019).
- [13] M. A. Caprio, P. J. Fasano, P. Maris, and A. E. McCoy, Quadrupole moments and proton-neutron structure in  $p$ -shell mirror nuclei, *Phys. Rev. C* **104**, 034319 (2021).
- [14] P. Maris, H. M. Aktulga, S. Binder, A. Calci, Ü. V. Çatalyürek, J. Langhammer, E. Ng, E. Saule, R. Roth, J. P. Vary, and C. Yang, No core CI calculations for light nuclei with chiral 2- and 3-body forces, *J. Phys. Conf. Ser.* **454**, 012063 (2013).
- [15] A. D'Alessio, T. Mongelli, M. Arnold, S. Bassauer, J. Birkhan, I. Brandherm, M. Hilcker, T. Hüther, J. Isaak, L. Jürgensen, T. Klaus, M. Mathy, P. von Neumann-Cosel, N. Pietralla, V. Y. Ponomarev, P. C. Ries, R. Roth, M. Singer, G. Steinhilber, K. Vobig, and V. Werner, Precision measurement of the  $E2$  transition strength to the  $2_1^+$  state of  ${}^{12}\text{C}$ , *Phys. Rev. C* **102**, 011302 (2020).
- [16] M. A. Caprio and P. J. Fasano, *Ab initio* estimation of  $E2$  strengths in  ${}^8\text{Li}$  and its neighbors by normalization to the measured quadrupole moment, *Phys. Rev. C* **106**, 034320 (2022).
- [17] H. Li, D. Fang, H. J. Ong, A. M. Shirokov, J. P. Vary, P. Yin, and X. Zhao, Quadrupole dynamics of carbon isotopes and  ${}^{10}\text{Be}$ , *Phys. Rev. C* **110**, 064325 (2024).
- [18] N. J. Stone, Table of nuclear electric quadrupole moments, *At. Data Nucl. Data Tables* **111–112**, 1 (2016).
- [19] I. Angeli and K. P. Marinova, Table of experimental nuclear ground state charge radii: An update, *At. Data Nucl. Data Tables* **99**, 69 (2013).
- [20] J. H. Kelley, J. E. Purcell, and C. G. Sheu, Energy levels of light nuclei  $A = 12$ , *Nucl. Phys. A* **968**, 71 (2017).
- [21] D. R. Tilley, C. M. Cheves, J. L. Godwin, G. M. Hale, H. M. Hofmann, J. H. Kelley, C. G. Sheu, and H. R. Weller, Energy levels of light nuclei  $A = 5, 6, 7$ , *Nucl. Phys. A* **708**, 3 (2002).
- [22] D. R. Tilley, J. H. Kelley, J. L. Godwin, D. J. Millener, J. E. Purcell, C. G. Sheu, and H. R. Weller, Energy levels of light nuclei  $A = 8, 9, 10$ , *Nucl. Phys. A* **745**, 155 (2004).
- [23] J. H. Kelley, E. Kwan, J. E. Purcell, C. G. Sheu, and H. R. Weller, Energy levels of light nuclei  $A = 11$ , *Nucl. Phys. A* **880**, 88 (2012).
- [24] F. Ajzenberg-Selove, Energy levels of light nuclei  $A = 13–15$ , *Nucl. Phys. A* **523**, 1 (1991).
- [25] C. Cockrell, J. P. Vary, and P. Maris, Lithium isotopes within the *ab initio* no-core full configuration approach, *Phys. Rev. C* **86**, 034325 (2012).
- [26] R. F. Casten, *Nuclear Structure from a Simple Perspective*, 2nd ed., Oxford Studies in Nuclear Physics No. 23

- (Oxford University Press, Oxford, 2000).
- [27] D. J. Rowe, *Nuclear Collective Motion: Models and Theory* (World Scientific, Singapore, 2010).
- [28] A. Bohr, The coupling of nuclear surface oscillations to the motion of individual nucleons, *Mat. Fys. Medd. Dan. Vid. Selsk.* **26** (1952).
- [29] M. A. Caprio, P. Maris, and P. J. Fasano, Robust *ab initio* predictions for dimensionless ratios of  $E2$  and radius observables. I. Electric quadrupole moments and deformation (2024), arXiv:2409.03926 [nucl-th].
- [30] W. J. Vermeer, M. T. Esat, J. A. Kuehner, R. H. Spear, A. M. Baxter, and S. Hinds, Electric quadrupole moment of the first excited state of  $^{12}\text{C}$ , *Phys. Lett. B* **122**, 23 (1983).
- [31] J. Saiz-Lomas, M. Petri, I. Y. Lee, I. Syndikus, S. Heil, J. M. Allmond, L. P. Gaffney, J. Pakarinen, H. Badran, T. Calverley, D. M. Cox, U. Forsberg, T. Grahn, P. Greenlees, K. Hadyńska-Klęg, J. Hilton, M. Jenkinson, R. Julin, J. Konki, A. O. Macchiavelli, M. Mathy, J. Ojala, P. Papadakis, J. Partanen, P. Rahkila, P. Ruotsalainen, M. Sandzelius, J. Sarén, S. Stolze, J. Uusitalo, and R. Wadsworth, The spectroscopic quadrupole moment of the  $2_1^+$  state of  $^{12}\text{C}$ : A benchmark of theoretical models, *Phys. Lett. B* **845**, 138114 (2023).
- [32] M. A. Caprio, P. J. Fasano, and P. Maris, Robust *ab initio* prediction of nuclear electric quadrupole observables by scaling to the charge radius, *Phys. Rev. C* **105**, L061302 (2022).
- [33] S. Pastore, S. C. Pieper, R. Schiavilla, and R. B. Wiringa, Quantum Monte Carlo calculations of electromagnetic moments and transitions in  $A \leq 9$  nuclei with meson-exchange currents derived from chiral effective field theory, *Phys. Rev. C* **87**, 035503 (2013).
- [34] D. J. Millener, Structure of unstable light nuclei, *Nucl. Phys. A* **693**, 394 (2001).
- [35] D. J. Millener, Hypernuclear gamma-ray spectroscopy and the structure of  $p$ -shell nuclei and hypernuclei, in *Topics in Strangeness Nuclear Physics*, Lecture Notes in Physics, Vol. 724, edited by P. Bydžovský, J. Mareš, and A. Gal (Springer, Berlin, 2007) p. 31.
- [36] M. A. Caprio, P. J. Fasano, P. Maris, A. E. McCoy, and J. P. Vary, Probing *ab initio* emergence of nuclear rotation, *Eur. Phys. J. A* **56**, 120 (2020).
- [37] P. Maris, M. Sosonkina, J. P. Vary, E. Ng, and C. Yang, Scaling of *ab-initio* nuclear physics calculations on multicore computer architectures, *Procedia Comput. Sci.* **1**, 97 (2010); M. Shao, H. M. Aktulga, C. Yang, E. G. Ng, P. Maris, and J. P. Vary, Accelerating nuclear configuration interaction calculations through a preconditioned block iterative eigensolver, *Comput. Phys. Commun.* **222**, 1 (2018).
- [38] P. J. Fasano, *Ab initio nuclear structure and electroweak properties from chiral effective field theory*, Ph.D. thesis, University of Notre Dame (2023).
- [39] A. M. Shirokov, I. J. Shin, Y. Kim, M. Sosonkina, P. Maris, and J. P. Vary, N3LO  $NN$  interaction adjusted to light nuclei in *ab exitu* approach, *Phys. Lett. B* **761**, 87 (2016).
- [40] A. M. Shirokov, J. P. Vary, A. I. Mazur, and T. A. Weber, Realistic nuclear Hamiltonian: *Ab exitu* approach, *Phys. Lett. B* **644**, 33 (2007).
- [41] E. Epelbaum, H. Krebs, and U.-G. Meißner, Precision nucleon-nucleon potential at fifth order in the chiral expansion, *Phys. Rev. Lett.* **115**, 122301 (2015).
- [42] E. Epelbaum, H. Krebs, and U.-G. Meißner, Improved chiral nucleon-nucleon potential up to next-to-next-to-next-to-leading order, *Eur. Phys. J. A* **51**, 53 (2015).
- [43] R. B. Wiringa, V. G. J. Stoks, and R. Schiavilla, Accurate nucleon-nucleon potential with charge-independence breaking, *Phys. Rev. C* **51**, 38 (1995).
- [44] S. C. Pieper, The Illinois extension to the Fujita-Miyazawa three-nucleon force, in *New Facet of Three Nucleon Force — 50 Years of Fujita Miyazawa Three Nucleon Force (FM50): Proceedings of the International Symposium on New Facet of Three Nucleon Force*, AIP Conf. Proc. No. 1011, edited by H. Sakai, K. Sekiguchi, and B. F. Gibson (AIP, New York, 2008) pp. 143–152.
- [45] C. Forssen, J. P. Vary, E. Caurier, and P. Navrátil, Converging sequences in the *ab-initio* no-core shell model, *Phys. Rev. C* **77**, 024301 (2008).
- [46] See Supplemental Material at <http://xxxxxxx> for comprehensive plots and tabulations of the calculated observables, as functions of  $N_{\max}$  and  $\hbar\omega$ .
- [47] B. Pritychenko, M. Birch, B. Singh, and M. Horoi, Tables of  $E2$  transition probabilities from the first  $2^+$  states in even-even nuclei, *At. Data Nucl. Data Tables* **107**, 1 (2016).
- [48] E. A. McCutchan, C. J. Lister, S. C. Pieper, R. B. Wiringa, D. Seweryniak, J. P. Greene, P. F. Bertone, M. P. Carpenter, C. J. Chiara, G. Gürdal, C. R. Hoffman, R. V. F. Janssens, T. L. Khoo, T. Lauritsen, and S. Zhu, Lifetime of the  $2_1^+$  state in  $^{10}\text{C}$ , *Phys. Rev. C* **86**, 014312 (2012).
- [49] E. A. McCutchan, C. J. Lister, R. B. Wiringa, S. C. Pieper, D. Seweryniak, J. P. Greene, M. P. Carpenter, C. J. Chiara, R. V. F. Janssens, T. L. Khoo, T. Lauritsen, I. Stefanescu, and S. Zhu, Precise electromagnetic tests of *ab initio* calculations of light nuclei: States in  $^{10}\text{Be}$ , *Phys. Rev. Lett.* **103**, 192501 (2009).
- [50] M. Freer, E. Casarejos, L. Achouri, C. Angulo, N. I. Ashwood, N. Curtis, P. Demaret, C. Harlin, B. Laurent, M. Milin, N. A. Orr, D. Price, R. Raabe, N. Soić, and V. A. Ziman,  $\alpha : 2n : \alpha$  molecular band in  $^{10}\text{Be}$ , *Phys. Rev. Lett.* **96**, 042501 (2006).
- [51] H. G. Bohlen, T. Dorsch, Tz. Kokalova, W. von Oertzen, Ch. Schulz, and C. Wheldon, Structure of  $^{10}\text{Be}$  from the  $^{12}\text{C}(^{12}\text{C}, ^{14}\text{O})^{10}\text{Be}$  reaction, *Phys. Rev. C* **75**, 054604 (2007).
- [52] D. Suzuki, A. Shore, W. Mittig, J. J. Kolata, D. Bazin, M. Ford, T. Ahn, D. Becchetti, S. Beceiro Novo, D. Ben Ali, B. Bucher, J. Browne, X. Fang, M. Febraro, A. Fritsch, E. Galyaev, A. M. Howard, N. Keeley, W. G. Lynch, M. Ojaruega, A. L. Roberts, and X. D. Tang, Resonant  $\alpha$  scattering of  $^6\text{He}$ : Limits of clustering in  $^{10}\text{Be}$ , *Phys. Rev. C* **87**, 054301 (2013).
- [53] Y. Kanada-En'yo, H. Horiuchi, and A. Doté, Structure of excited states of  $^{10}\text{Be}$  studied with antisymmetrized molecular dynamics, *Phys. Rev. C* **60**, 064304 (1999).
- [54] P. J. Li *et al.*, Validation of the  $^{10}\text{Be}$  ground-state molecular structure using  $^{10}\text{Be}(p, pa)^6\text{He}$  triple differential reaction cross-section measurements, *Phys. Rev. Lett.* **131**, 212501 (2023).
- [55] M. A. Caprio, P. J. Fasano, A. E. McCoy, P. Maris, and J. P. Vary, *Ab initio* rotation in  $^{10}\text{Be}$ , *Bulg. J. Phys.* **46**, 445 (2019).
- [56] M. A. Caprio, A. E. McCoy, P. J. Fasano, and T. Dytrych, Symmetry and shape coexistence in  $^{10}\text{Be}$ , *Bulg. J. Phys.* **49**, 57 (2022).

- [57] A. S. Davydov and G. F. Filippov, Rotational states in even atomic nuclei, *Nucl. Phys.* **8**, 237 (1958).
- [58] E. K. Warburton, J. W. Olness, K. W. Jones, C. Chasman, R. A. Ristinen, and D. H. Wilkinson, Lifetime determinations for nuclei  $A = 10, 11$ , and  $12$  from gamma-ray Doppler shifts, *Phys. Rev.* **148**, 1072 (1966).
- [59] T. R. Fisher, S. S. Hanna, D. C. Healey, and P. Paul, Lifetimes of levels in  $A = 10$  nuclei, *Phys. Rev.* **176**, 1130 (1968).
- [60] A. M. Lane, Reduced widths of individual nuclear energy levels, *Rev. Mod. Phys.* **32**, 519 (1960).
- [61] S. Raman, C. W. Nestor, Jr., and P. Tikkanen, Transition probability from the ground to the first-excited  $2^+$  state of even-even nuclides, *At. Data Nucl. Data Tables* **78**, 1 (2001).
- [62] J. Hiura and I. Shimodaya, Alpha-particle model for  ${}^9\text{Be}$ , *Prog. Theor. Phys.* **30**, 585 (1963); Errata: Alpha-particle model for  ${}^9\text{Be}$ , *Prog. Theor. Phys.* **31**, 165 (1964).
- [63] S. Okabe, Y. Abe, and H. Tanaka, The structure of  ${}^9\text{Be}$  nucleus by a molecular model. I, *Prog. Theor. Phys.* **57**, 866 (1979); S. Okabe and Y. Abe, The structure of  ${}^9\text{Be}$  nucleus by a molecular model. II, *Prog. Theor. Phys.* **61**, 1049 (1979).
- [64] M. Seya, M. Kohno, and S. Nagata, Nuclear binding mechanism and structure of neutron-rich Be and B isotopes by molecular-orbital model, *Prog. Theor. Phys.* **65**, 204 (1981).
- [65] W. von Oertzen, Two-center molecular states in  ${}^9\text{B}$ ,  ${}^9\text{Be}$ ,  ${}^{10}\text{Be}$ , and  ${}^{10}\text{B}$ , *Z. Phys. A* **354**, 37 (1996).
- [66] W. von Oertzen, Dimers based on the  $\alpha + \alpha$  potential and chain states of carbon isotopes, *Z. Phys. A* **357**, 355 (1997).
- [67] M. Freer, The clustered nucleus—cluster structures in stable and unstable nuclei, *Rep. Prog. Phys.* **70**, 2149 (2007).
- [68] Y. Kanada-En'yo and H. Horiuchi, Opposite deformations between protons and neutrons in proton-rich C isotopes, *Phys. Rev. C* **55**, 2860 (1997).
- [69] T. Suhara and Y. Kanada-En'yo, Quadrupole deformation  $\beta$  and  $\gamma$  constraint in a framework of antisymmetrized molecular dynamics, *Prog. Theor. Phys.* **123**, 303 (2010).
- [70] S. Shen, S. Elhatisari, D. Lee, U. Meißner, and Z. Ren, *Ab initio* study of the beryllium isotopes  ${}^7\text{Be}$  to  ${}^{12}\text{Be}$  (2024), arXiv:2411.14935 [nucl-th].
- [71] P. Maris, *Ab initio* nuclear structure calculations of light nuclei, *J. Phys. Conf. Ser.* **402**, 012031 (2012).
- [72] M. A. Caprio, A. E. McCoy, and P. J. Fasano, Intrinsic operators for the translationally-invariant many-body problem, *J. Phys. G* **47**, 122001 (2020).
- [73] Z.-T. Lu, P. Mueller, G. W. F. Drake, W. Nörtershäuser, S. C. Pieper, and Z.-C. Yan, Laser probing of neutron-rich nuclei in light atoms, *Rev. Mod. Phys.* **85**, 1383 (2013).
- [74] A. E. McCoy, M. A. Caprio, P. Maris, and P. J. Fasano, Intruder band mixing in an *ab initio* description of  ${}^{12}\text{Be}$ , *Phys. Lett. B* **856**, 138870 (2024).